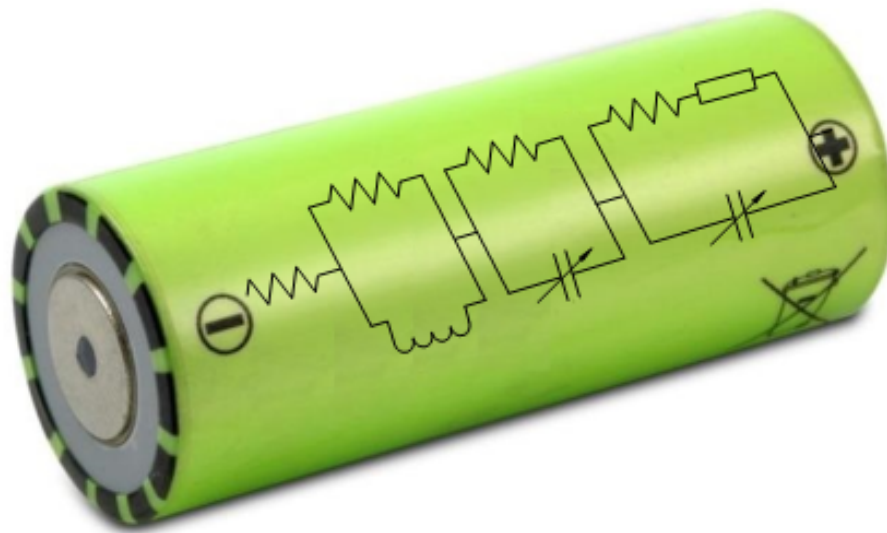


CHALMERS



Modeling of Ageing of Lithium-Ion Battery at Low Temperatures

Master of Science Thesis

AVNISH NARULA

Department of Energy and Environment
Division of Electric Power Engineering
CHALMERS UNIVERSITY OF TECHNOLOGY
Göteborg, Sweden 2014

The Volvo logo, consisting of the word "VOLVO" in white, bold, sans-serif capital letters on a dark blue rectangular background.

Modeling of Ageing of Lithium-Ion Battery at Low Temperatures

AVNISH NARULA

Department of Energy and Environment
Division of Electric Power Engineering
CHALMERS UNIVERSITY OF TECHNOLOGY
Göteborg, Sweden 2014

Modeling of Ageing of Lithium-Ion Battery at Low Temperatures
AVNISH NARULA

© AVNISH NARULA, 2014.

Department of Energy and Environment
Division of Electric Power Engineering
Chalmers University of Technology
SE-412 96 Göteborg
Sweden
Telephone +46 (0)31-772 1000

Chalmers Bibliotek, Reproservice
Göteborg, Sweden 2014

Abstract

For mass production of HEVs, performance characteristics and prediction of ageing behaviour of Lithium-ion batteries is essential. This thesis considers the performance and durability of the battery system to be used in commercial Hybrid Electric Vehicles. The purpose of the work presented in this thesis is to link capacity fading to battery usage and to investigate how low temperature conditions and charging rates affect the cycle life and ageing processes of batteries developed for use in HEVs.

Ten $LiFePO_4$ //Graphite cells optimized for power applications were systematically aged using a simple charge-discharge cycle with constant current rate spanning multiple C-rates (1C, 2C and 4C) and temperatures ($0^\circ C$, $-10^\circ C$ and $-15^\circ C$). Extensive impedance spectroscopy tests were conducted in order to build equivalent circuit model of the cell. The experimental impedance spectra of the positive electrode and the fitted one show good agreement for all the cases up to a SoC range of 10%-80%

Lithium loss was found to be the dominant ageing mechanism for most of the test cases. A CC/CV charge and a CC discharge even with active air cooling was *not* found to be a suitable approach at a low temperature of $-15^\circ C$ due to dramatic self heating of the cells. A wide SoC range was found to have a profound effect on ageing.

Index Terms: Hybrid Electric Vehicles, Lithium-ion battery, battery testing, battery model, state of health, impedance spectroscopy

*“The stone age came to an end not for lack of stones
And the oil age will come to an end not for the lack of oil”
– Sheikh Yamani, Former Saudi oil minister*

Acknowledgements

The following people, companies and institutions have contributed significantly to this thesis or supported throughout the project. I would like to thank

- my mother, father and friends for their encouragements and empathy,
- my supervisor, Jens Groot and my examiner Prof. Torbjörn Thiringer for having made this project possible and for their support and patience,
- Volvo Group Trucks Technology, Advanced Technology & Research for letting me use their battery testers and other equipments,
- Azra Selimovic, Director, Electromobility sub-systems, Volvo GTT, AT&R, for letting me carry out this work in her group,
- Sophie Tintignac, Ylva Olofsson, Istaq Ahmed and Timofey Maltsev from Volvo GTT for their help and patience,
- Adam Einarsson, for helping me with L^AT_EX.

Avnish Narula
Göteborg, Sweden, 2014

Contents

Abstract	iii
Acknowledgements	v
Contents	vii
List of Symbols & Abbreviations	ix
1 Introduction	1
1.1 Problem definition, purpose and requirements	1
1.1.1 Problem description	1
1.1.2 Purpose and requirements	2
1.2 Battery Terminology	2
1.3 Previous Work	3
1.4 Thesis Scope	3
2 Li-Ion batteries	5
2.1 Electrode materials for Lithium-ion batteries today	5
2.2 <i>LiFePO₄</i> – Cathode material considered	6
2.3 Lithium-Ion Batteries : Performance Comparison	7
3 Ageing mechanism in the Li-ion cell	9
3.1 Lithium-ion System	9
3.2 Solid Electrolyte Interphase (SEI)- Main ageing mechanism	9
3.3 Review of work in battery modeling	10
3.3.1 Impedance based models with ageing	10
3.3.2 Electrochemical models with ageing	11
4 Model Selection	13
4.1 Semi-physical impedance based model	13
4.2 Equivalent circuit based model	14
5 Data Collection	15
5.1 Test Sequence Overview	15
5.2 Formation Tests	16
5.3 Reference Performance Tests	17
5.4 Electrochemical Impedance Spectroscopy	19
5.5 Cycle life Test Procedure	20

5.5.1	Proposed Load Cycle profile	21
5.5.2	Test Conditions	22
6	Model Analysis	23
6.1	Determination of Open Circuit Voltage (OCV)	23
6.2	Electrochemical Impedance Spectroscopy	24
6.2.1	Model Structure	24
6.2.2	Fitted Parameter Analysis	28
6.2.3	Model Validation	29
7	Cell Ageing Analysis	31
7.1	Impedance Spectroscopy Comparison	31
7.2	Temperature Distribution	32
7.3	Cycling measurements results: Stress Factor Dependence	34
7.3.1	Capacity Fading: Temperature dependence	34
7.3.2	Capacity Loss at room temperature	36
7.4	Comparison of Open Circuit Voltage for different tests	37
7.5	Voltage Profiles	38
8	Conclusions & Future Work	41
8.1	Conclusion	41
8.2	Future work	41
	References	43
	A Specifications	47
	B Test Conditions	49
	C Calculations	51
	C.1 Linear Least-Squares Regression	51
	C.1.1 R^2 : Coefficient of determination	51
	D Open Circuit Voltage	53
	D.1 OCV Model Parameters	53
	E Proposed Model	55
	F Weighted least-square parameter estimation	57
	G Impedance Based Circuit Model Parameters	59

List of Symbols & Abbreviations

ΔZ_{imag}	Difference between real part of simulated and measured impedance multiplied by a chosen weight vector
ΔZ_{real}	Difference between real part of simulated and measured impedance multiplied by a chosen weight vector
ΔZ	Total error
C_{dl}	Double layer capacitance
C_l	Long time transient capacitance
C_{SEI}	Capacitance of the surface film layer on the electrodes
C_s	Short time transient capacitance
R_b	Bulk resistance of the cell
R_{ct}	Charge transfer resistance
R_l	Long time transient resistance
R_{ohm}	Ohmic resistance
R_{SEI}	Resistance of the surface film layer on the electrodes
R_s	Short time transient resistance
Z_w	Warburg's impedance
Z_{exp}	Measured impedance
Z_{sim}	Simulated impedance
AC	Alternating Current
BEV	Battery Electric Vehicle
BoL	Beginning of Life
CC	Constant current charge or discharge
CPE	Constant Phase Element
cte	close-to-equilibrium
CV	Constant voltage charge or discharge

Contents

DC	Direct Current
DEC	Diethyl Carbonate
DMC	Dimethyl Carbonate
EC	Ethylene Carbonate
EIS	Electrochemical Impedance Spectroscopy
EMF	Electromotive Force
EoL	End of Life
GTT	Volvo Group Trucks Technology
HEV	Hybrid Electric Vehicle
ISO	International Organization for Standardization
LFP	<i>LiFePO₄</i> ; Lithium Iron Phosphate
NLLS	Nonlinear Least Squares
OCV	Open Circuit Voltage
PC	Personal Computer
PHEV	Plug-in Hybrid Electric Vehicle
RC	Residual Capacity
RPT	Reference Performance Test
SEI	Solid Electrolyte Interphase
SoC	State of Charge

Chapter 1

Introduction

With the increasing concerns of vehicle emissions and competition between major automobile manufacturers, electric and hybrid electric vehicles have carved a niche for themselves [1]. The advancements in the development of batteries has lead to a substantial production of electric powered vehicles up to a range of 450 km [2]. However, the introduction of these vehicles is not going smoothly due to a lacking charging infrastructure, long charging times and the high purchase price. Most importantly, it is unknown how electric vehicles and their battery behave in the long run and what their rest value will be [3].

1.1 Problem definition, purpose and requirements

Lithium-ion batteries are being used in commercial electrical vehicles since 2009 and their use in vehicles is increasing very rapidly. Still there remains a substantial amount of work regarding the ageing modeling of batteries. As these batteries are more and more deployed for transportation applications, assurances of lifetime and reliability are essential [4].

This thesis is part of a project which aims to understand the ageing mechanisms of a Li-ion battery system used in HEV (*Hybrid Electric Vehicle*) powertrains [5]. With a battery model, the behaviour of the battery can be predicted and the rest value of the battery can be determined more accurately [3].

First, the problems will be identified and defined. To investigate the problem for the specific application, the aim and requirements of the work will be given. Since in battery research, many ambiguous terms exist, the terms used in this thesis will be defined. Then the scope of the thesis will be defined, as battery modelling is a very extensive field.

1.1.1 Problem description

As temperatures drop below freezing point ($-20\text{ }^{\circ}\text{C}$ - $+10\text{ }^{\circ}\text{C}$), full power is not available when the battery is at low temperature and as a consequence, a significant amount of the electrical vehicle's performance can be lost. Trying to charge the battery at the same rate that is possible during warm conditions can shorten the battery life. The ageing processes leads to a drastically increased internal resistance, reduced power capability and capacity decrease. Sub-zero temperature conditions

are also the reason to consider ordering an extended range battery pack even if it comes as an additional price for the vehicle.

1.1.2 Purpose and requirements

The desired result of this work is to link capacity fading to battery usage, to investigate what modification in charging current rate that is possible at subzero temperature conditions and to predict if low temperature testing can be performed at relevant load conditions. Since the most interesting things happen at the intersection of disciplines, this thesis has been written from the point of view of a battery user and electrical engineer.

1.2 Battery Terminology

In this section, the terms used in this thesis will be defined. These definitions are in accordance with British and European Standards unless otherwise specified.

State-of-Charge (SoC)

State-of-Charge is commonly defined as the ratio between the amount of charge stored in the battery to the amount of charge that can be stored when the battery is fully charged [6].

End of Life (EoL)

End of Life is a condition reached when the device under test is no longer capable of meeting the applicable goals [7]. It is often defined as the state when the device under test degrades to 80% of its initial capacity.

State-of-Health (SoH)

It is the present fraction of allowable performance deterioration remaining before EoL. (SOH = 100% at beginning of life and 0% at end of life)

C-rate

The C-rate is the current normalized with the battery capacity stated by manufacturer at the reference conditions. That is, a 1,000 mAh battery which is discharged at 1 C-rate (C/1) should ideally deliver the full capacity in one hour. A 10 C-rate (C/0.1) will charge/discharge the battery in 0.1 hour and 0.25 C-rate (C/4) will discharge the battery in 4 hours [5] [8].

Cycle

A sequence of a discharge followed by a charge or a charge followed by a discharge under specified conditions.

Open Circuit Voltage (OCV_{cte})

The Open Circuit Voltage of a cell is the voltage of the cell when it is at electrochemical equilibrium. Depending on the battery size, type and State-of-Charge, the time to reach electrochemical equilibrium varies strongly. For a simple charge-discharge cycle, the close to equilibrium open circuit voltage can be mathematically described by (1.1).

$$OCV_{cte} = \frac{V_{charge} + V_{discharge}}{2} \quad (1.1)$$

Equation 1.1 is applicable when the possible hysteresis effect of the OCV_{cte} is ignored and it is considered temperature independent. *cte* is the close-to equilibrium condition.

Residual Capacity (RC)

The residual capacity is the capacity that is left in a battery after an apparent full discharge at a given condition. The RC is the maximum total capacity minus the Full Charge Capacity [9].

1.3 Previous Work

Extensive work has been done in the area of battery modeling and it can be concluded that there is not one general model of Li-ion cells. Many types of battery models were found in literature including electrochemical models, fractional discharge battery models, dynamic lumped parameters battery models (equivalent circuit based models), as well as hydrodynamic, and finite element models (electrochemical models based on COMSOL).

Electrochemical models: Electrochemical models provide detailed physics based information about the Li-ion batteries.

Equivalent Circuit based models: Equivalent circuit based models such as proposed by Hu et al. [6] is often selected because of its simplicity and universal acceptance.

Impedance based models: These models are based on the frequency analysis and allows to separate different internal processes and estimate the parameters in the form of a semi-physical equivalent circuit model using measurements from the electrochemical impedance spectroscopy measurement data.

1.4 Thesis Scope

Due to extensiveness in the battery modelling research, a scope must be defined to limit this thesis to some specific operating conditions and application. In this thesis, an equivalent circuit based ageing model will be implemented with focus on single Li-ion cells for resistance increase and capacitance decrease and the obtained values

of the circuit components will be related to the electrochemical processes in the cells. The chosen Li-ion chemistry in this work is $LiFePO_4//Graphite$. Approximately 10 cells will be tested under realistic, but accelerating operating conditions. The specific ageing factor which is of interest in this work is charging at at low temperature ($-15\text{ }^\circ\text{C} - +0\text{ }^\circ\text{C}$).

Chapter 2

Li-Ion batteries

For an energy storage material, the amount of charge that can be stored in a material per unit of mass is crucial. This property is usually called specific capacity. Also, a high potential ensures the requirement of fewer cells for a battery of given voltage. Lithium is an attractive material for batteries with the lowest potential (-3.05 V) *vs.* hydrogen and the highest specific capacity (3.86 Ah/g) [2]. Apart from many applications in laptops (2.5 billion cells/year), iPods, eReaders and smartphones which are all powered by lithium batteries, the third element in the periodic table (Lithium) may also hold the key to an environmentally sustainable future [1].

2.1 Electrode materials for Lithium-ion batteries today

Many electrode materials are used in the commercial Lithium-ion batteries. It may be noted that systems with metallic lithium are not used in EV & HEV applications. Some of the electrode materials are listed in Tables 2.1 and 2.2.

Table 2.1 Cathode materials for Li-ion batteries.

Cathode Material	Specific Capacity[mAh/g]	Notes/Comments
<i>LiCoO₂</i>	140	Good lifetime High safety risk
<i>LiFePO₄</i>	170	Cheap and safe
<i>LiMn₂O₄</i>	125	Cheaper, safety better than for Co and Ni
<i>LiNiO₂</i>	200	High safety risk Good performance
<i>NMC</i>	170-250	Popular material from automotive perspective
<i>LiNi_{1/3}Mn_{1/3}Co_{1/3}O₂</i>	145	Popular material

Table 2.2 Anode materials for Li-ion batteries.

Anode Material	Specific Capacity [mAh/g]	V vs. Li/Li ⁺	Notes/ Comments
Hard Carbon (LiC_6)	500	0.4	Small number of full cycles
Silicium ($Li_{22}Si_6$)	4250	0.4-0.6	High energy density
Graphite(LiC_6)	280	0.1-1.0	Expensive, high Number of full cycles
Titanate ($Li_4Ti_5O_{12}$)	150	1.55	Safe, low energy density, potential is significantly above Li potential
Lithium (Li)	4000	0-0.3	

In theory, any combination of cathode and anode can be used in rechargeable Li-ion cells although $LiFePO_4$ and Titanate will give a very low voltage of 1.2 V. This combination, however could be good for stationary applications [10]. $LiCoO_2$ has the best lifetime among all candidates. The automotive industry wants to get rid of Co since it is expensive and poisonous. Candidates like $LiNi_{1/3}Mn_{1/3}Co_{1/3}O_2$ have made it easier to realise since it offers a wide range of variability for optimizing proportions. Candidate *NMC* is most popular right now from automotive perspective. The proportion can be varied by having 5% of Co and the remaining is something else [11]. It can be an interesting blend of Lithium Cobalt Oxide and *NMC*. All of the above combinations have pros and cons regarding performance and lifetime.

2.2 $LiFePO_4$ – Cathode material considered

This thesis work is a part of an ongoing research project. Therefore, there was no scope for the choice of cathode and anode material. The cathode material for the cells tested is $LiFePO_4$. The material is known to be developed for having high power and high charging rate. It has good stability and lifetime and has more tolerance for overcharging. *LFP* is not an energy material but a power material. That is why it is used in HEVs and PHEVs (Plug-in Hybrid Electric Vehicles). It is quite easy to replace 12 V Pb-Acid battery by a new $LiFePO_4$ battery and is a possible material for ‘second generation’ in vehicles which means that batteries can be charged for re-use time and time again. The material has high thermal stability and is called more *safe* material. Though the material has some issues to address as well. The calendaric lifetime is not very clear and the diagnostics is very difficult. The material is also known to have sluggish lithium diffusion kinetics.

The salt used in the electrolyte is $LiPF_6$ in different solvents, usually EC+DEC and EC+DMC. Fluorides are needed to get stability into the batteries. It has been reported in [12] that $LiPF_6$ in the electrolyte generates fewer types of layer forming salts and smoother Li deposition compared to $LiAsF_6$ and $LiClO_4$ inhibiting the dendrite occurrence and extending the battery life.

2.3 Lithium-Ion Batteries : Performance Comparison

The success of Lithium-ion battery is mainly due to its significant advantages in terms of performance. A common way of comparing the performance of different battery technologies is to have one performance attribute on the vertical axis and another performance attribute on the horizontal axis.

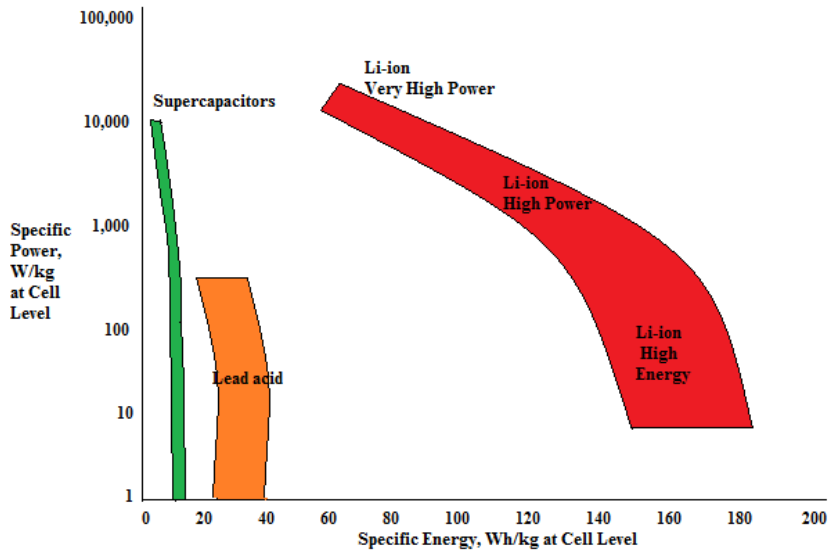


Figure 2.1 The Ragone plot of various cell types capable meeting the requirements for HEV applications.

It can be seen in Figure 2.1 that the lithium-ion technology performs better than lead-acid or nickel-metal hydride (NiMH) cells in terms of both energy and power for a given battery weight. This means that lithium-ion cells exhibit very good power performance. It can also be seen that, for very high power requirement, capacitors are more suitable than electrochemical batteries but the energy storage capabilities of capacitors are very limited.

Chapter 3

Ageing mechanism in the Li-ion cell

Li-ion batteries are complex systems to understand, and the study of ageing is even more complicated [13]. The process of degradation results from several underlying processes occurring in the cell during cycling or storage [14]. However, the performance degradation during cycling usually occurs much faster than storage under the same conditions [3].

In this chapter, to understand the degradation mechanism of Li-ion battery, firstly the operation of the Li-ion system will be explained. As mentioned in the purpose in section 1.1, the degradation phenomenon is linked to capacity fading, accordingly, here the degradation mechanism will be described.

3.1 Lithium-ion System

The anode material in a lithium-ion battery is usually graphite and the cathode material is typically either $LiFePO_4$ or NMC . The particles on both electrodes, though mainly on anode (graphite), are covered with a surface film, which is called Solid Electrolyte Interphase. The electrolyte can be solid, polymer or liquid and is a central component regarding low temperature and lifetime performance [15]. The separator is an expensive sub-component in Li-ion cell and avoids short-circuits. The Li-ions go back and forth i.e. charge and discharge. As each Li-ion comes across, there is an equivalent electron going in the external circuit. Every electron that goes through the load is accompanied by the Li-ion in the battery as shown in Figure 3.1. When the battery is cycled, the Li-ions move back and forth; hence the battery stores energy and releases it continuously in every cycle.

3.2 Solid Electrolyte Interphase (SEI)- Main ageing mechanism

The main ageing process in the Li-ion system can be explained by the loss of Li-ions to the layer formation. On the negative active material surface, a passivating layer is created. The layer formation initiated by contact of the electrode with the solutions consists of the partially soluble and insoluble reduction components of the

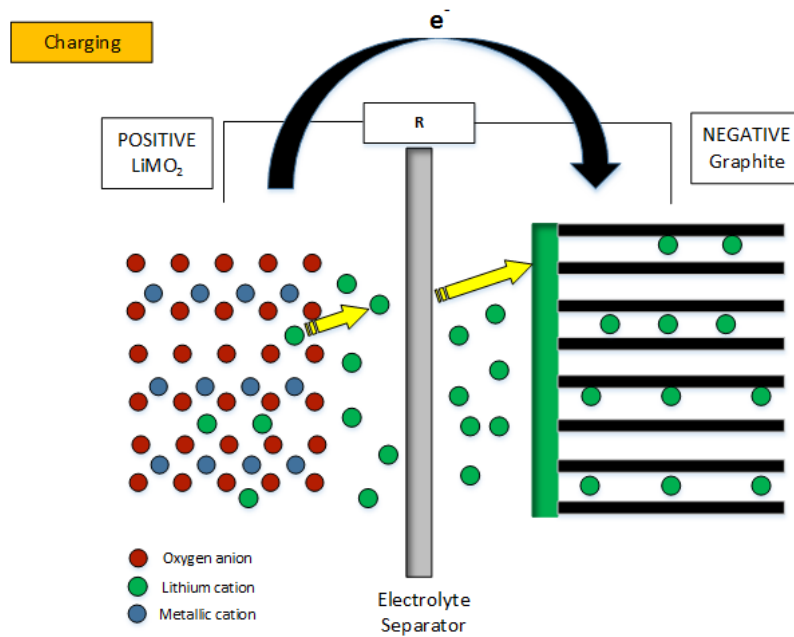


Figure 3.1 A schematic representation of Li-ion battery cell.

electrolyte and is created during fast charging process as well as during low-current cycling. The cell characteristics are influenced by the *SEI* since Li ions have to pass through it. The thickening of this layer leads to even higher internal resistance [16]

Most significant mechanisms of power fade/impedance rise are summarized below [5]:

1. Surface film formation of both electrodes with low conductivity
2. Loss of electrode area and electrode material leading to a higher local current density
3. Lower diffusivity of lithium ions into active electrode particles and slower kinetics (increased charge transfer resistance) due to surface films
4. Reduced conductivity between particles due to both surface films and degradation of binders, possibly in combination with a binder-Li reaction
5. Loss of cyclable Lithium

3.3 Review of work in battery modeling

3.3.1 Impedance based models with ageing

The low temperature behaviour of a *LiCoO₂* cell has been reported in [17]. The impedance-based model was similar to the other impedance-based models, with an inductance-resistance pair added to the circuit. From experiments the ohmic resistance was found to be invariant with the temperature, whereas the polarisation resistance follows the Arrhenius equation. With the use of Randles circuit, the obtained impedances can be related to electrochemical processes in the cell, which is shown in Figure 3.2. The polarisation resistance is split into R_{SEI} and R_{ct} , where

R_{SEI} was nearly invariant with the SoC and R_{ct} strongly dependent on the SoC. The activation energy of R_{SEI} at high SoC was different than lower SoCs, but nearly invariant for R_{ct} . An equation for the temperature dependence of R_{ct} was obtained with the Butler-Volmer equation. This behaviour at low temperatures was confirmed by Zhang et al for a nickel-based mixed oxide cathode Li-ion cell [18] and a commercial $LiCoO_2$ cell. R_{ct} became significant higher than the ohmic resistance and R_{SEI} at low temperatures, especially at low SoC. This could lead to charging difficulties at low temperatures.

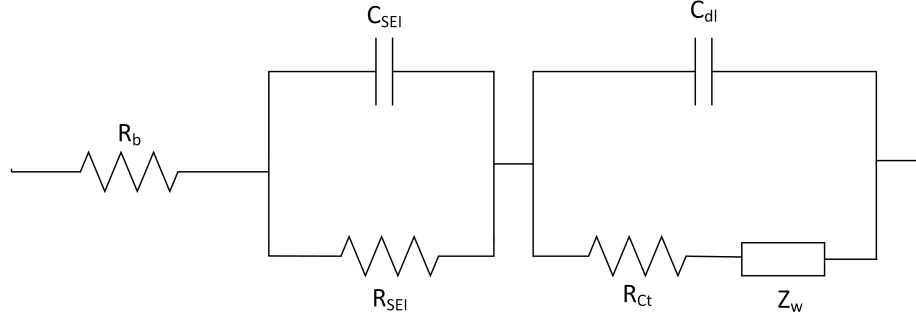


Figure 3.2 An example of the circuit elements identified in the AC response in the Randles Circuit [17].

3.3.2 Electrochemical models with ageing

Tippmann et al [19] have developed a pseudo-2D electrochemical model to understand internal processes and predicting ageing effects. The model was applied to a wide range of temperature ($T = -25^\circ C$ to $40^\circ C$) and current (0.1 C to 6 C) coupled with a 0 D thermal model. Capacity fade was measured after a significant number of cycles and compared to the simulated anode potential. A qualitative correlation was found between the degradation in an experiment and the anode potential dropping below 0 V. At this condition, a mechanism called lithium plating is noticed which occurs when the electric potential of the anode reaches zero.

Chapter 4

Model Selection

Section 3.3 focused on the review of work in the battery modeling. This chapter will focus on the selected model.

4.1 Semi-physical impedance based model

Figure 4.1 represents the semi-physical impedance based model which can explain the complex electrochemical conversion process in the battery. The circuit can be compared to the 2nd order Randle based circuit but due to the presence of Warburg's impedance, the Randles circuit is complex in simulation realization [20].

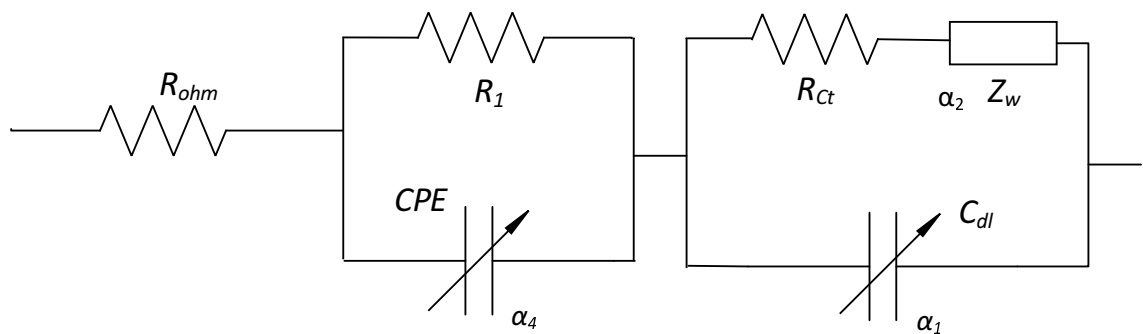


Figure 4.1 Semi-physical impedance based model.

In literature, a number of modeling approaches were found to model the Warburg's impedance with the transfer functions having frequency dependence. But the work in [5] suggests that a constant phase element is equally good or better so the Warburg's impedance can be modelled as a constant phase element. Theoretically, a constant phase element is a really large semicircle. The choice of the transfer function in general depends on how low in frequency, the user wants to go. Since in this work, the lowest frequency chosen is 10 mHz , a constant phase element is a good choice. In Figure 4.1, the Warburg's impedance Z_w is modelled as a constant phase element with a constant phase of 45° representing the diffusion of the lithium ions between the active material and the electrolyte and corresponds to the low frequency response in the spectroscopy measurement. It has been reported in [21] that charge transfer phenomena and diffusion phenomena occur in distinct frequency regions

and as a result the time constant of both processes can be considered to differ by at least one order of magnitude.

The charge transfer resistance R_{ct} is related to the charge transfer between the electrolyte and electrode. C_{DL} is the capacitance between the electrolyte and the electrode. These two components account for the response in the medium frequency range (100mHz to 10kHz) [3].

4.2 Equivalent circuit based model

Electrical circuit based models are comprehensively used in engineering applications. In this thesis, an intuitive equivalent circuit model with a resistor-capacitor parallel network has been used. Figure 4.2 shows the equivalent circuit based model which consists of an electromotive force (EMF), V_{oc} as a dependent voltage source which is a function of the state of charge in series with the resistor-capacitor parallel network. The ohmic resistance of the battery cell is given by R_{ohm} , which includes the bulk resistance R_b and surface layer resistance R_{SEI} . R_s and C_s represent the short time constants in the voltage response, which is related to the charge transfer resistance R_{ct} and double layer capacitance C_{dl} . The long time transient time constants are accounted for by R_l and C_l , which is linked to a single RC pair Warburg impedance equivalence modelling the diffusion phenomena. A problem is that the equivalent circuit model must match the real battery data at all temperatures.

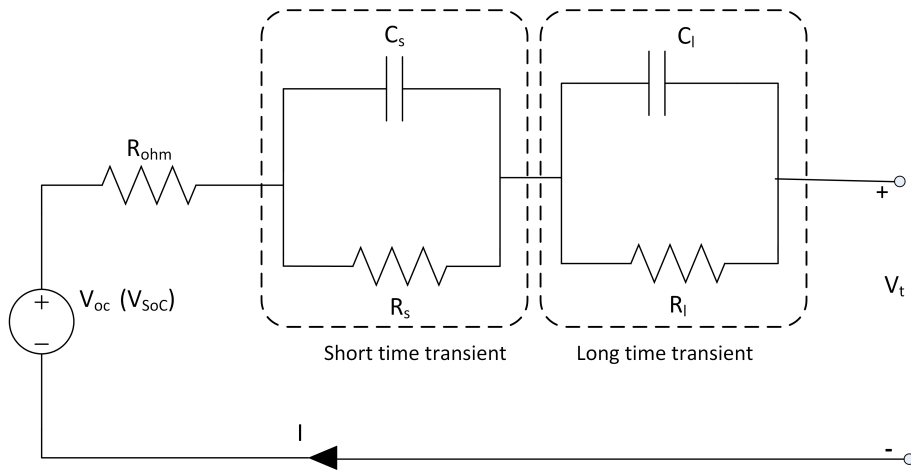


Figure 4.2 An equivalent circuit based model adapted from [22].

Chapter 5

Data Collection

In Chapter 4 (*Model Selection*), the proposed circuit based model was described. In this chapter, the experimental setup will be discussed. The test sequence consists of a number of procedures including formation tests, reference performance tests, electrochemical impedance spectroscopy tests and cycle life tests.

The subsequent sections describe the test setup used in the procedures. The general procedures described comply with the ISO standards. The data set considered in this project was collected at the battery ageing laboratory at Volvo Group Trucks Technology, Advanced Technology & Research and Chalmers University of Technology.

5.1 Test Sequence Overview

The test sequence plan is presented in Figure 5.1. With this plan, the aim was to age the cells significantly during a limited period. The different test sub-procedures have been explained in more detail in subsequent sections.

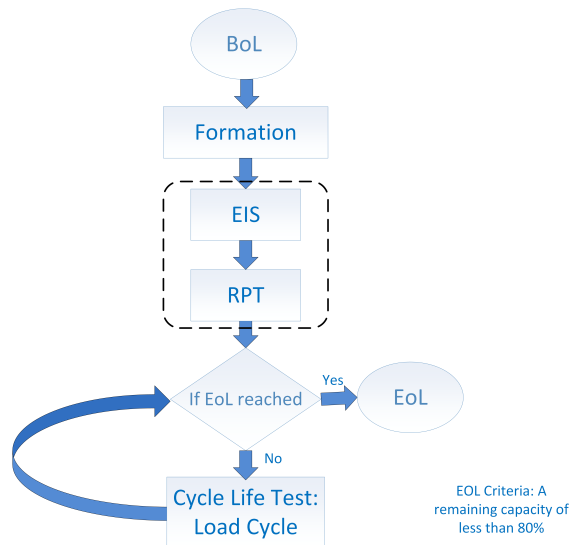


Figure 5.1 Flowchart of test sequence plan from BoL to EoL including RPT and EIS tests and cycle life test

(BoL: Beginning of Life, EoL: End of Life, RPT: Reference Performance Test, EIS: Electrochemical Impedance Spectroscopy).

5.2 Formation Tests

The test procedure started with a Beginning of Life (BoL) formation test consisting of five charge-discharge cycles and to ensure that the rated capacity is reached and that the performance is stabilised. A 15 minute pause was introduced between every charge and discharge cycle. This was to ensure that the cell temperature is close to the ambient (rest) temperature before each step is started.

The experimental setup consists of the following components: multiple $LiFePO_4$ cells, energy source, test procedure controller and programmer and a data logger. The setup is shown in Figure 5.2. The formation tests were done on a *Digatron* battery tester/simulator. The battery tester serves as the energy source, measurement equipment and test procedure controller. The cell under testing is a four-year old A123 System Li-ion rechargeable ANR26650 cell [23]. The specification of the cell can be found in Table A.1 in Appendix A.

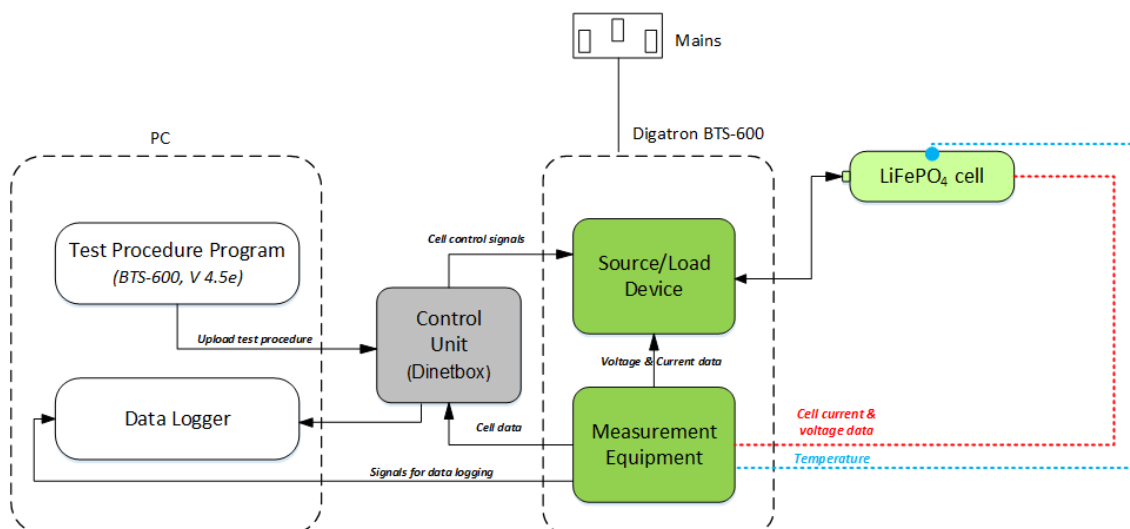


Figure 5.2 Experimental setup for Formation Test.

The Digatron BTS-600 battery tester has two independent channels. The technical specifications can be found in Table A.3 in Appendix A. Each channel can be programmed with its own test procedure, which is run from the battery tester. The programming of the battery tests is done into the software BTS-600 and uploaded to the battery tester. The battery tester logs the data on its own internal memory. The actual temperature was measured with a thermoelectric in the top of the cell and was installed with adhesive directly onto it. All cell tests have been performed using a custom made cell holder shown in Figure 5.3 with a four wire connection and an individual cell monitoring.

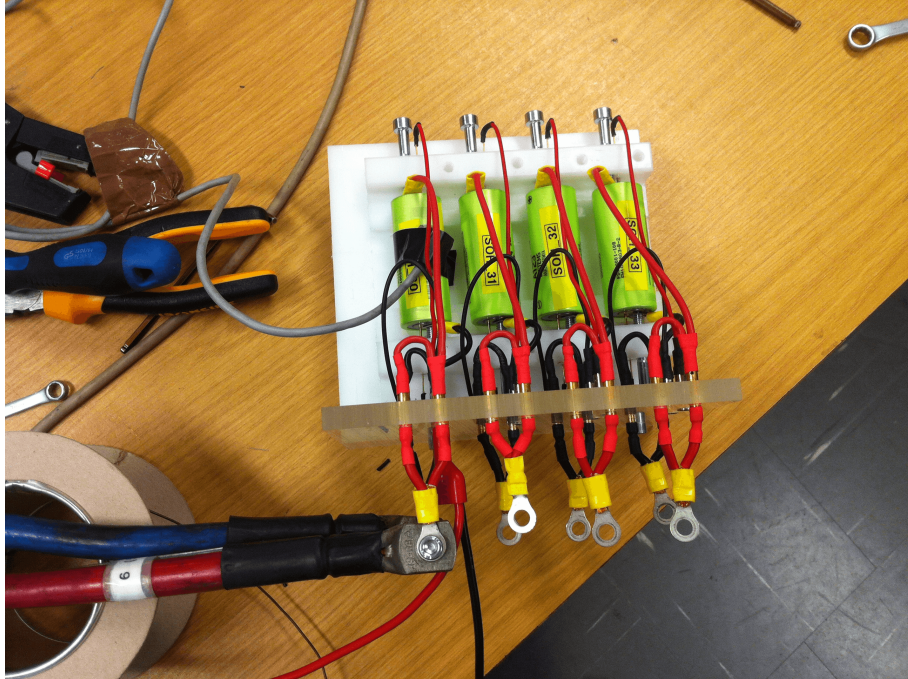


Figure 5.3 Custom made cell holder with four wire connection.

5.3 Reference Performance Tests

Reference Performance Tests (RPTs) are a set of tests performed at periodic intervals during life testing to establish the condition and rate of performance degradation of devices under test. Such tests are performed periodically during life testing of a cell, as well as at the start- and end-of-life testing [24]. They are trade-offs between getting the required data and adding potential ageing to the cell.

The tests were performed on a *Maccor* equipment at 24°C. The specifications for the equipment can be found in Table A.4 in Appendix A. Like for *Digatron* equipment, each channel in the *Maccor* equipment can be programmed with its own test procedure, which is run from a test PC.

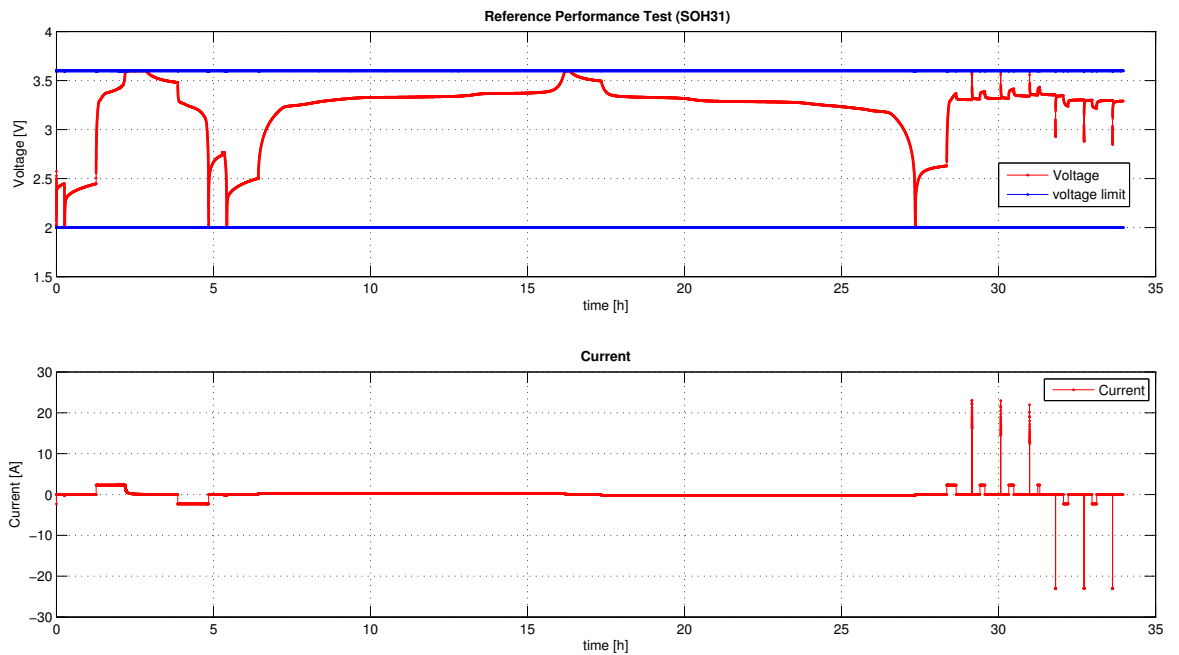
A customized RPT procedure developed in [5] was used in this thesis. A one hour rest period was chosen between each charge and discharge so the cells would reach the electrochemical equilibrium. The procedure is explained in Table 5.1, performed at 24°C.

The definition of 0% state of charge in step 0 was defined according to the manufacturer's defined minimum safe voltage which was 2 V for the particular cells used in these experiments. A similar maximum safe voltage of 3.6 V was also specified by the manufacturer [23]. Charging was performed with a constant current (CC) and is followed by a constant voltage (CV) until the current drops below a specific value. As break criteria for the CV phase $I < C/20$ was chosen. This formed the definition of 100% SoC. Once minimum voltage was reached, the controller was alerted to stop discharging the cell.

Table 5.1 Reference Performance Test Procedure.

Step	Step Description	Notes/Comments
0	Discharge to 0% SoC	Residual capacity test
1	Charge and discharge at $1C$ rate	$1C$ capacity test: Charge and Discharge
2	Charge and discharge at $C/10$ rate	Voltage profile and Capacity at low current rate. Used for calculating OCV
3	Charge Power test at $10C$ rate	Charge power tests at 30, 50 and 70% SoC
4	Discharge Power test at $10C$ rate	Discharge tests at 80, 60 and 40% SoC

The measurements were taken at every 30 seconds or whenever the voltage was changing with 10 mV . Charge power tests were performed at 30, 50 and 70% SoC and discharge tests at 80, 60 and 40% SoC as done in previous work [5]. The voltage and current data recorded during one of these reference performance tests is shown below in Figure 5.4.

**Figure 5.4** Reference Performance test at 24°C .

From the reference performance test data, the open-circuit voltage (OCV) of the cell was determined by the test cycle. The data points were taken at every 0.25% SoC. The data was fitted using non-linear least squares method in Matlab using *nlinfit* and the fit of close to equilibrium open circuit voltage (cte-OCV) was determined.

5.4 Electrochemical Impedance Spectroscopy

The poor power performance of the Li-ion battery at low temperature is due to the slow kinetics of the electrode reactions [25]. Frequency analysis allows to separate different internal processes; therefore to analyse the electrode kinetics of the cell, Electrochemical Impedance Spectroscopy (EIS) measurement on the cell was performed. A GAMRY® instrument was used for measurements in Hybrid EIS mode which is a blend of potentiostatic and galvanostatic mode.

The impedance response of the cell was measured at a frequency range of 10mHz to 50kHz at 10mV rms , $22\text{-}24^\circ\text{C}$ for SoC levels of 20%, 40% and 60% (for Beginning of life) and for SoC levels ranging from 10%-90% for End of Life. With the obtained measurements, Nyquist plots where the imaginary part of the impedance is plotted against the real part were obtained, the value of each circuit component in Randles circuit were determined for the conditions the cell was measured at. Each circuit component corresponds to one or more electrochemical processes in the cell and the model becomes more accurate when a higher order Randles circuit is used.

Fig. 5.5 shows 4-wire connection setup of reference and working sense electrodes. Figure 5.6 shows the connection setup used in the laboratory.

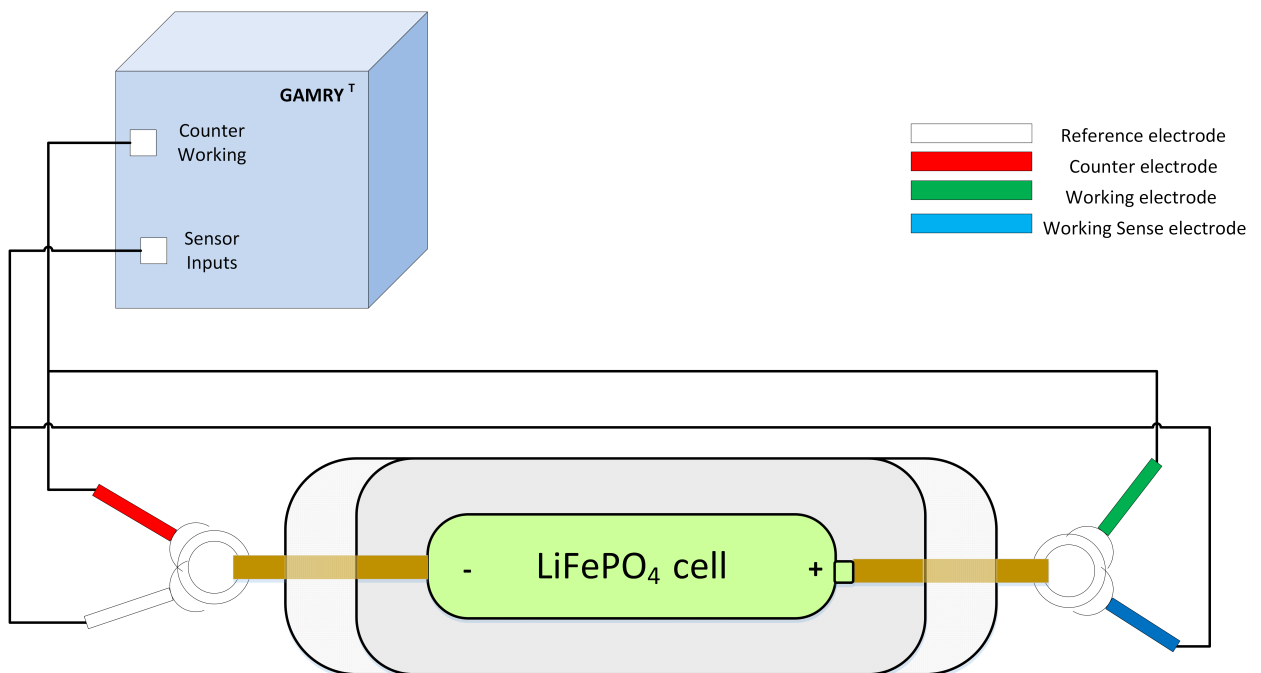


Figure 5.5 Experimental setup for Spectroscopy test.



Figure 5.6 Experimental setup for Spectroscopy test.

The GAMRY Instruments Reference 3000 software was used to realize the test setup which has also been summarized in Table B.1 in Appendix B. Table 5.2 summarizes the test procedure used for BoL tests in the laboratory.

Table 5.2 Electrochemical Impedance Spectroscopy Programme for BOL at 24°C.

Step	Step Description
0	Open Circuit Potential
1	Discharge Curve
2	Open Circuit Potential
3	Begin Loop (3 cycles)
3.0	Charge Curve
3.1	Open Circuit Potential
3.2	Hybrid EIS
3.3	Open Circuit Potential
4	End Loop

5.5 Cycle life Test Procedure

This section explains the cycle used for the cycle life tests for the cells. The ageing mechanism of a Li-ion battery is a complex mechanism and is rarely dependent on one phenomenon. To test the influence of various stress factors on a Li-ion cell, each cell was tested under a different temperature and C-rate level. The test setup is shown in Figure 5.7.

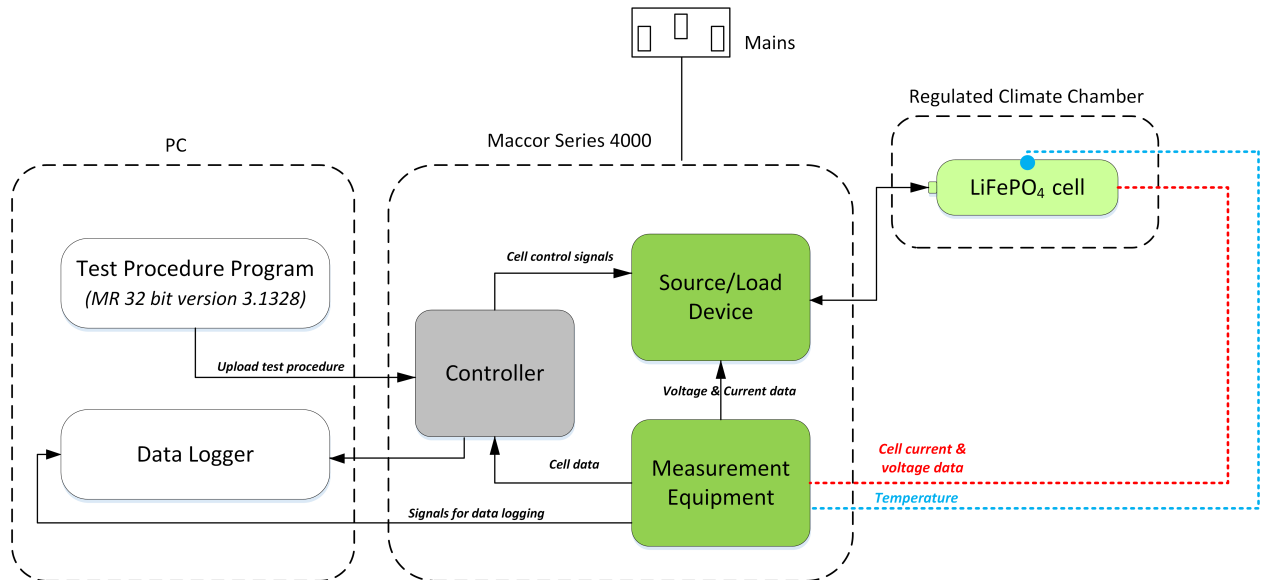


Figure 5.7 Test set up for Cycle Life test.

5.5.1 Proposed Load Cycle profile

The actual level of CC charging in a Li-ion cell depends on whether the cell is power optimized or energy optimized. In this thesis, a simple charge-discharge cycle with constant current rate was used to characterize the ageing of the battery which consists of a constant current discharge step immediately followed by a constant current / constant voltage charge step. The SoC range in such cycle is usually wide which has a profound effect on ageing [5]. Figure 5.8 shows the battery ageing profile and voltage response for one of the test cases.

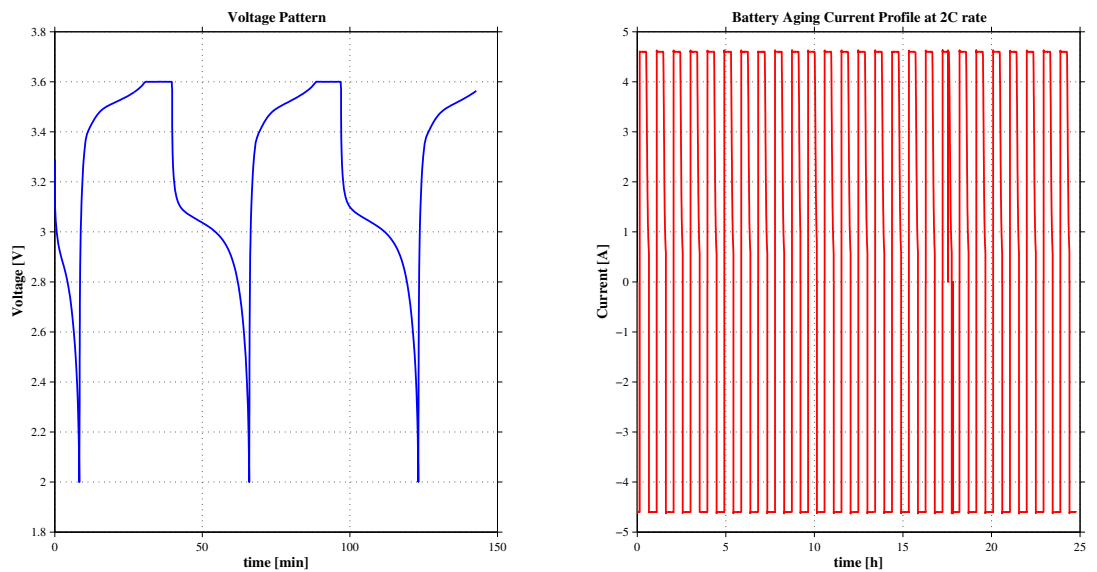


Figure 5.8 Battery ageing current profile and voltage response
Example: 2C/2C test.

5.5.2 Test Conditions

Each test condition aims to investigate the influence of one stress factor. At the time of the experiments, two channels were available to be subjected to different test conditions. The cycle life test was performed on 9 cells¹ (4 cell pairs at different C-rates ($1C$, $2C$ and $4C$) and temperatures ($0\text{ }^{\circ}C$, $-10\text{ }^{\circ}C$ and $-15\text{ }^{\circ}C$) and a cell at room temperature ($+23\text{ }^{\circ}C$)). Test data for Case R was collected from previous work [5]. The *Test Conditions/Stress Factor* will be explained in detail in Chapter 7.

Table 5.3 The test procedures conducted with each cell.

Case	C-rate discharge	C-rate charge	Temperature	Test Conditions/ Stress Factor	Cycles run
A1	2 C	2 C	0°C	Average cycling temperature of 5°C	300
A2	2 C	2 C	0°C	Average cycling temperature of 5°C	300
B1	2 C	2 C	-10°C	Average cycling temperature of -3°C	150
B2	2 C	2 C	-10°C	Average cycling temperature of -3°C	150
C1	2 C	2 C	-15°C	Self heating of the cells	100
C2	2 C	2 C	-15°C	Self heating of the cells	100
D1	4 C	4 C	0°C	Average cycling temperature of 15°C	150
D2	4 C	4 C	0°C	Average cycling temperature of 15°C	150
E1	4 C	4 C	-15°C	CC-CV in both directions with forced air cooling, self heating of the cells	100
R ²	1 C	1 C	+23°C	Reference Condition	4500

¹All tests were done with a CC/CV charge and a CC discharge except E1 which was CC-CV charge/discharge with forced air cooling

²This case was not conducted in the laboratory. The data was collected from previous work [5]

Chapter 6

Model Analysis

6.1 Determination of Open Circuit Voltage (OCV)

From literature [26], the OCV was found to be slightly dependent on the temperature and exhibits hysteresis. The OCV can then be described as

$$V_{oc}(SoC, T) = V_{oc,ref}(SoC) + \Delta V_{oc}(T) \quad (6.1)$$

An RPT was performed at $0^{\circ}C$ to check the temperature dependence of OCV. The close-to-equilibrium (cte) OCVs for discharging and charging were averaged to obtain the OCV as per 6.2. The averaged OCV for both the temperatures is shown in Figure 6.1.

$$OCV_{cte} = \frac{V_{charge} + V_{discharge}}{2} at C/10 \quad (6.2)$$

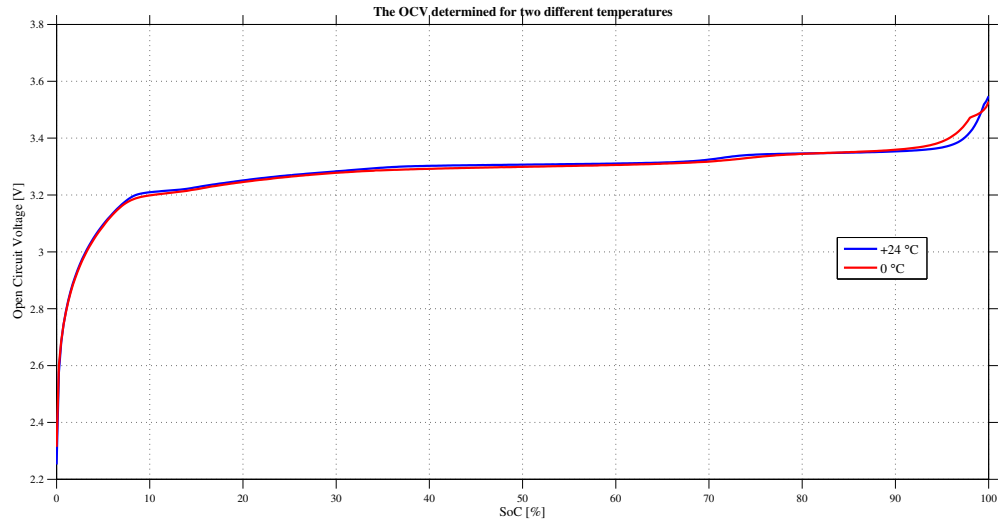


Figure 6.1 The OCV determined for two different temperatures ($24^{\circ}C$ & $0^{\circ}C$) for $C/10$ rate.

From Figure 6.1, the mean deviation from the reference temperature ($24^{\circ}C$) was found to be $8mV$. Since the temperature fluctuations were considerably small, the OCV is considered temperature independent. The possible hysteresis effect of the OCV is also ignored in this model, making it independent of the current direction. By measuring the close-to-equilibrium (cte) OCV as explained in section 5.3 for

discharging and charging, the OCV is modelled using the expression adapted from [27].

$$V_{oc}(SoC) = a_1 e^{-a_2 SoC} + a_3 + a_4 SoC + a_5 e^{\frac{a_6}{1-SoC}} \quad (6.3)$$

where a_1 to a_6 are all constants and V_{oc} is the Open Circuit Voltage. For this case, before the cell was aged, $a_1 = -0.72$, $a_2 = -0.41$, $a_3 = 3.22$, $a_4 = 1.77 \times 10^{-3}$, $a_5 = 0$ and $a_6 = 0$

The OCV has been determined by the procedure described in Table 5.1 and shown in Figure 5.4. The cells were rested for one hour during each interval.

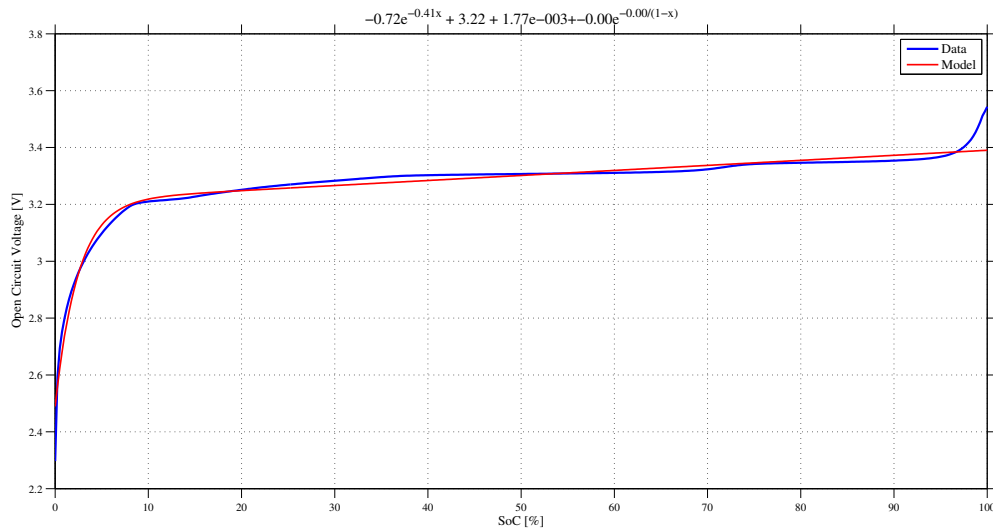


Figure 6.2 The OCV data at 24°C fitted with equation 6.3 for C/10 rate.

An adjusted R^2 of 0.96 was obtained indicating that the curve fit is reasonably accurate. R^2 was calculated based on the calculated residuals and the dependent variable (OCV). Method of calculations for R^2 is explained in Appendix C. The model parameters for all the cases have been summarized in chapter D in Table D.1 and Table D.2 for BoL and EoL respectively.

6.2 Electrochemical Impedance Spectroscopy

6.2.1 Model Structure

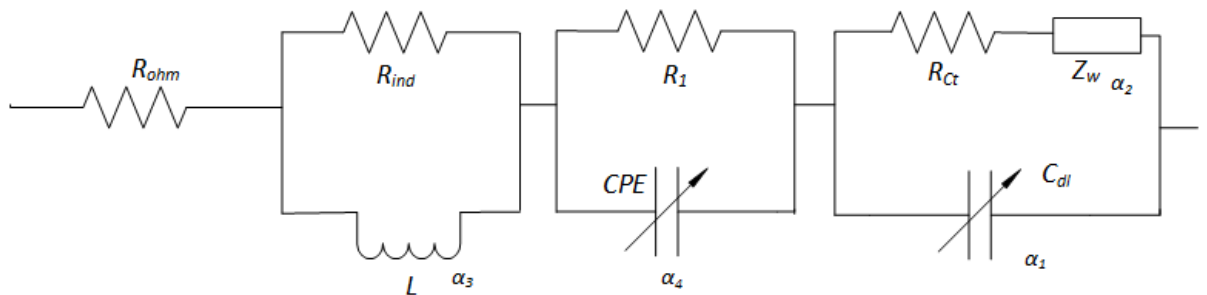
Various frequencies, particularly the lower ones, yield a more complete picture of battery health. The nyquist plots were obtained at a frequency range of 10 *mHz* to 50 *kHz*.

From the measured EIS, a number of key parameters were estimated from the semi-physical impedance based model using non-linear least squares method in Matlab mentioned in Table 6.1

Table 6.1 Key parameters estimated from the semi-physical impedance based model.

Component	Description	Notes/Comments
R_{ohm}	<i>Ohmic Resistance</i>	The intersection with the real axis of the impedance curve in the Nyquist graph (Resistance from electrode, electrolyte, separator and connection)
R_{ct}	<i>Charge Transfer Resistance</i>	The real impedance approximately at the position of the local minima in the <i>Nyquist</i> plot
$L + \alpha_3$	<i>Inductor</i>	High frequency inductance
R_{ind}	<i>Resistance in parallel to the inductor</i>	Resistance modelled to get a better fit to the data
$C_{dl} + \alpha_1$	<i>Double Layer Capacitance</i>	Modelled as a constant phase element.
$Z_w + \alpha_2$	<i>Warburg diffusion Impedance</i>	Modelled as a constant phase element.
R_1	<i>Auxiliary Resistance</i>	An auxiliary resistance for a better fit.
$CPE + \alpha_4$	<i>Capacitance</i>	Modelled as constant phase element.

Figure 6.3 shows the semi-physical impedance based model which consists of all the components listed in Table 6.1.

**Figure 6.3** Semi-physical impedance based model.

In general, in the electrochemical impedance spectrum, the first part appears as a part of a circle. Theoretically, a constant phase element is a large semicircle therefore the choice of constant phase element is good. The transfer functions [5] of the constant phase elements (*CPEs*) and the inductance is given by

$$Z_{CPE} = \frac{1}{(j\omega)^\alpha C} \quad (6.4)$$

$$Z_L = (j\omega)^\alpha L \quad (6.5)$$

where $0 < \alpha < 1$.

A pure inductance is a straight line in the impedance spectrum and a pure inductance with the term α origins from the same point but is bent and can be compared to a semicircle. Thus the choice of constant phase element to model this is an acceptable approach as given by (6.5)

The impedance parameters were determined by fitting the experimental spectra with (6.4) & (6.5) using a complex nonlinear least squares method. In practice, the Matlab function *fmincon* that determines the minimum of function ΔZ which is defined as

$$\Delta Z = (Z_{sim} - Z_{exp})^2 \quad (6.6)$$

was used to fit the experimental spectra. Therefore, the optimization problem becomes

$$\min \Sigma (Z_{sim} - Z_{exp})^2 \quad (6.7)$$

In the original optimization problem, the variables were quite different from each other. The ratio of the highest to the lowest optimization variable was found to be of the order of 10^5 . In this case, the optimizer *fmincon* always tries to optimize changes in the variable with high value and changes to it will cause big effect. Therefore, the solution to (6.7) was obtained by making every optimization variable of the same order of magnitude. The same was done for the objective function and then multiplying it by a weight to prioritize those that seem to be most critical. This procedure is called regularization of nonlinear least squares problems [28]. The procedure has been summarized in Appendix F.

The inductance added in the circuit was used to describe the positive reactance response at high frequencies. However, the high frequency measurements were excluded from the optimization process. Figure 6.4 shows the model fit and the spectroscopy measurements.

Based on lithium-ion battery impedance data and model structure, parameters of the circuit for one of the cases (Case A2) were calculated as given in Table 6.2.

Table 6.2 Simulated parameters for the Randle Circuit.

Parameter	Value	Unit
R_{ohm}	0.0024	Ω
R_{ct}	0.0024	Ω
L	6×10^{-7}	H
R_{ind}	0.81095	Ω
α_3	0.59826	-
Z_w	492.737	F
α_2	0.54	-
CPE	2	F
α_4	0.45	-
C_{dl}	8.63	F
α_1	0.45	-

The lithium-ion battery nyquist plot based on Randles circuit model is shown in Figure 6.4

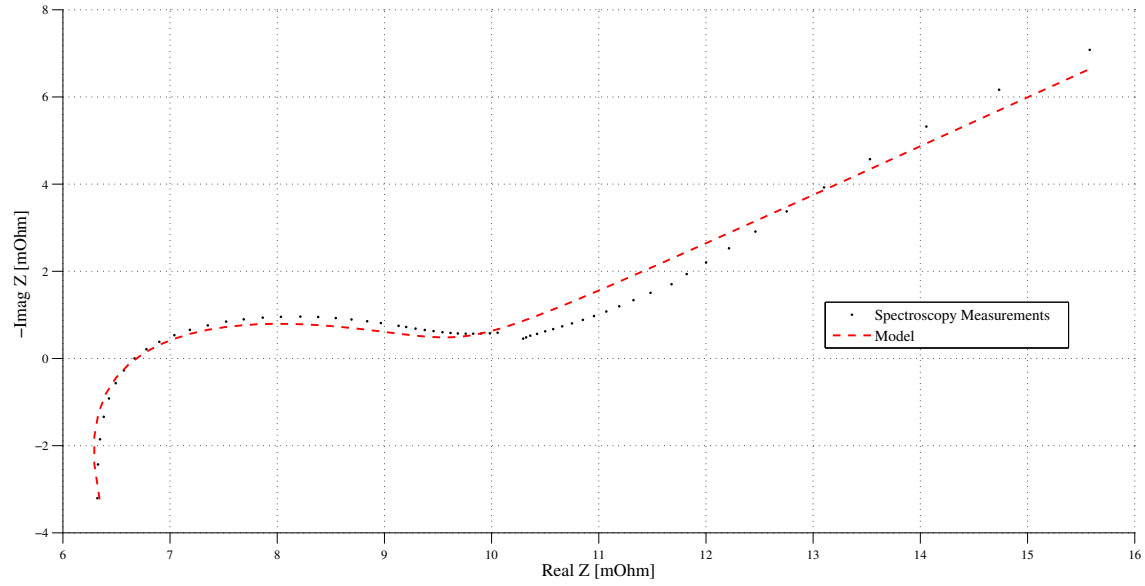


Figure 6.4 Spectroscopy measurements *vs.* model fit at 24°C .

6.2.2 Fitted Parameter Analysis

In this section, the fitted parameters (*Ohmic resistance, inductance and charge transfer resistance*) will be analysed.

Ohmic resistance and Inductance

A pure inductance is a straight line and a pure inductance with the term α as given by (6.5) will originate from the same point but is bent. If only pure inductance is considered, it will always reach zero for dc. Since the spectroscopy measurements were performed at 10 mV rms, the current setup doesn't have a DC hence small contribution of the real parts of the components to the overall resistance was found. Checking from the Spectroscopy measurement the ohmic resistance was found to be 6-7 m Ω and the ohmic resistance from the impedance based model was found to be in the range of 2 m Ω . Since the modelled inductance is a complex quantity, it has both real and imaginary part and therefore can be mathematically described as

$$(j\omega)^\alpha L = a + bj \quad (6.8)$$

Looking from a physical perspective of a cell, the whole ohmic resistance should have been in R_{ohm} . The inductance is more to compensate for the possible artefacts in the measurements. However, the inductance and the resistance R_{ind} modelled as a parallel pair had contributions to the overall ohmic resistance as shown in Figure 6.5 which agrees with the spectroscopy measurement data values.

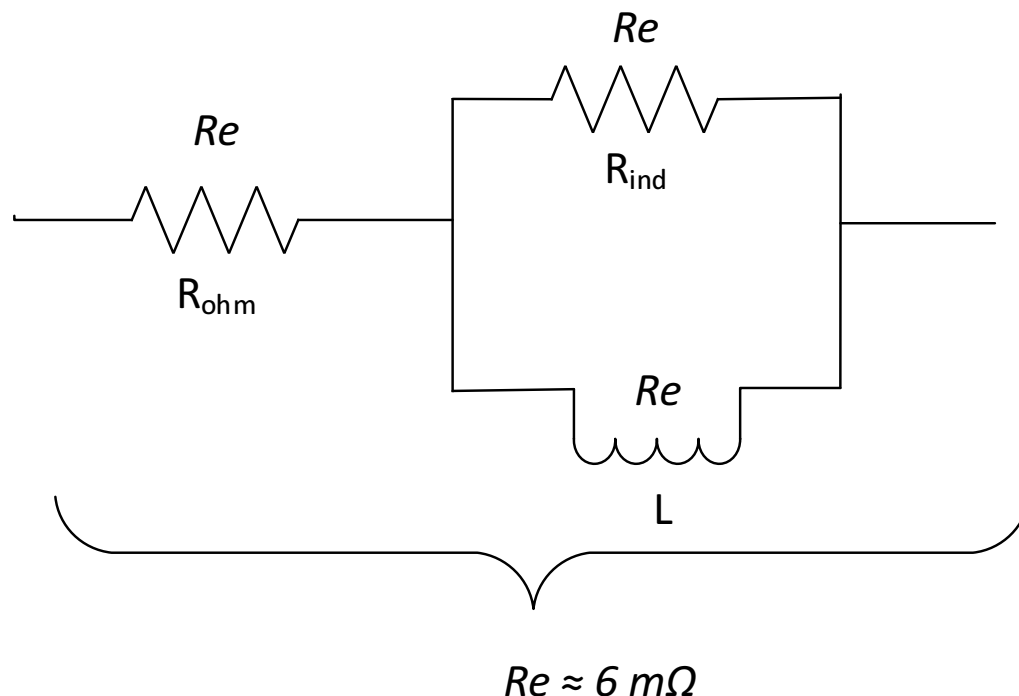


Figure 6.5 Contributions from other components to overall ohmic resistance (Re = Real) .

Further, the ohmic resistance after cycling the cells was found to be of the order

of milliohms and was independent of the State of Charge (SoC) in accordance with theory [9].

Charge transfer resistance

The charge-transfer resistance R_{ct} was found to be dependent on the SoC because it is related to the concentrations of active species and changes in mass transport properties [5].

6.2.3 Model Validation

The fitted parameter values for all the cases have been summarized in section G in Appendix D. The experimental impedance spectra of the positive electrode and the fitted one show good agreement for all the cases up to a SoC range of 10%-80% as illustrated in Figure 6.4 for one of the cases.

Chapter 7

Cell Ageing Analysis

7.1 Impedance Spectroscopy Comparison

Figure 7.1 shows the spectroscopy measurement results of fresh cells and the cells cycled at different temperatures and C rates mentioned in Table 5.3

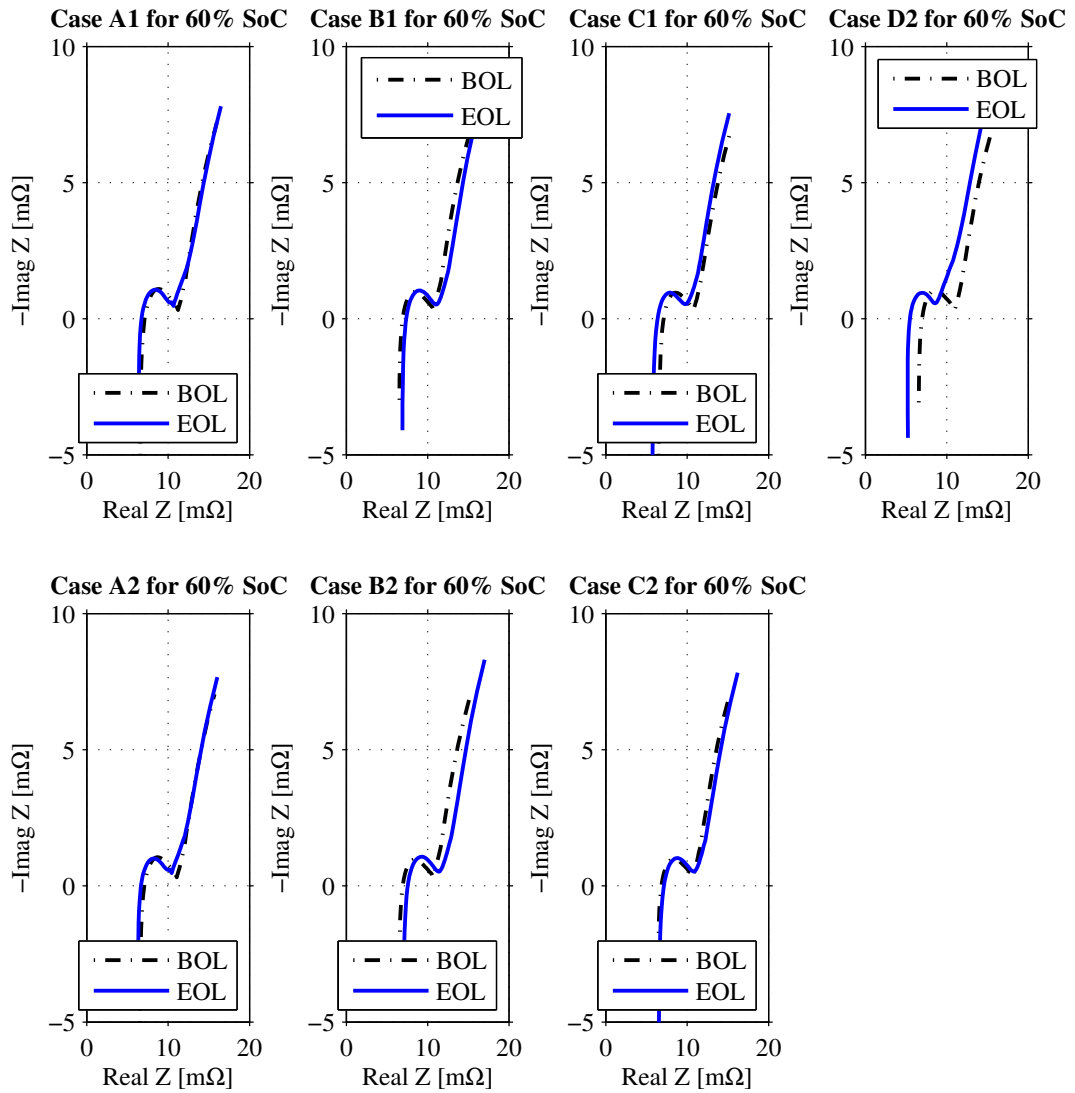


Figure 7.1 Spectroscopy Comparison of an aged cell with a non aged cell for 60% SoC .

Cases A1 and A2 show a decrease in ohmic resistance. Case D2 has a similar

behaviour which indicates that some cells improve for sometime in the initial few hundred cycles. Cases B1 and B2 show considerable increase in ohmic resistance which is a sign that Case B1 and B2 show more significant ageing. The breaks in between the measurements can be ascribed to the measurement disturbances due to the connecting cables.

7.2 Temperature Distribution

According to [29], for a small cylindrical cell, the temperature over the entire cell surface is almost constant except at the positive terminal, which shows a higher temperature. Figure 7.2 shows the minimum, maximum and average extracted surface temperature of the cells for different test cases in Table 5.3. The interesting case is D1 (0°C, 4C) where the maximum cell surface temperature was found to be 23°C (close to room temperature).

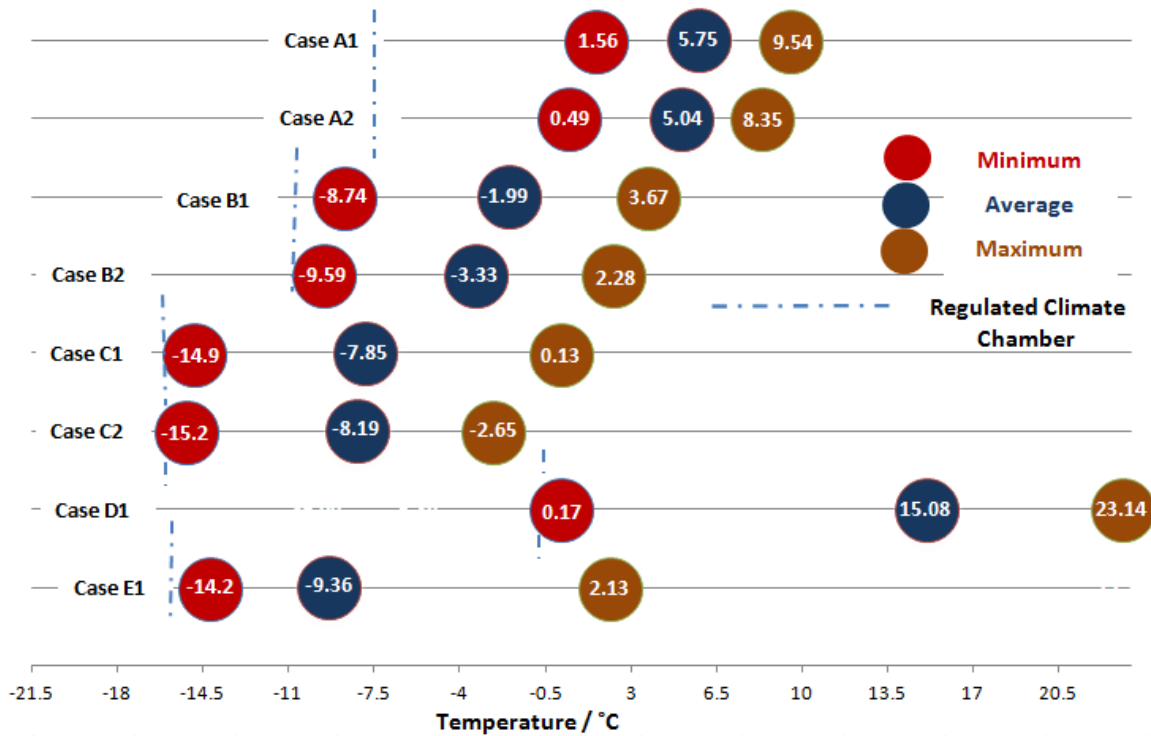


Figure 7.2 Temperature Distribution for cells for different tests described in Table 5.3.

Figures 7.3 - 7.5 show the temperature distribution as a function of cycle number for cases A1 to E1. The extracted minimum, maximum and average temperatures were found to be in close agreement with the minimum, maximum and average temperature spanning 20 cycles.

For instance, Figure 7.5 shows the temperature distribution as a function of cycle number for Cases C1 and C2. For Case C1, the mean temperature was found to be -7.83°C and for Case C2, the mean temperature was -8.3°C. The temperature values agree with the extracted average temperature measured continuously.

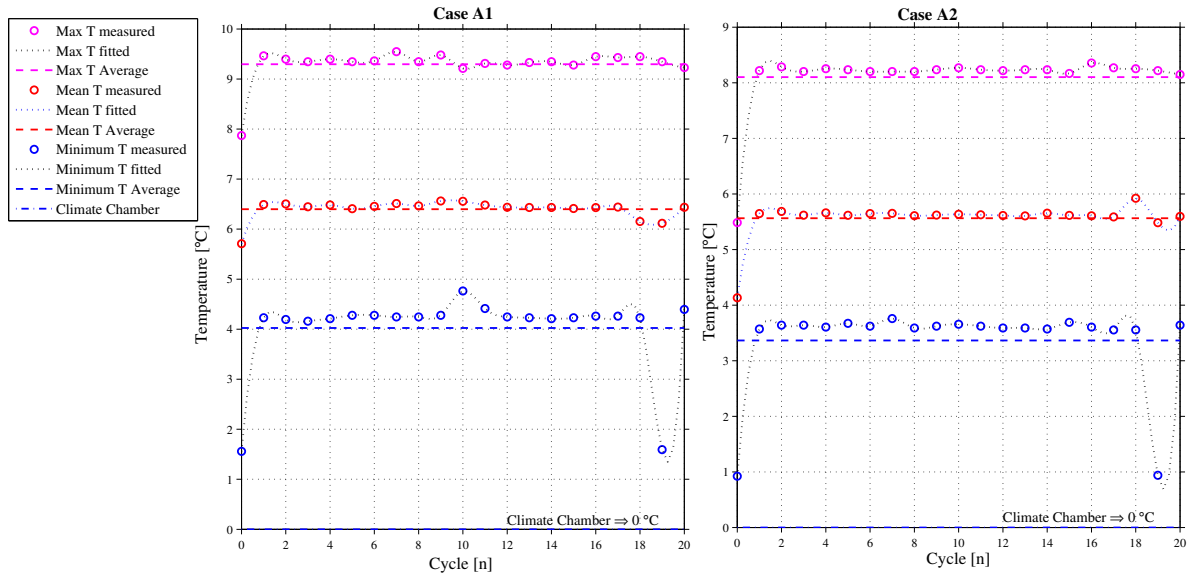


Figure 7.3 Temperature Distribution as a function of Cycle no. for Cases A1 and A2 described in Table 5.3.

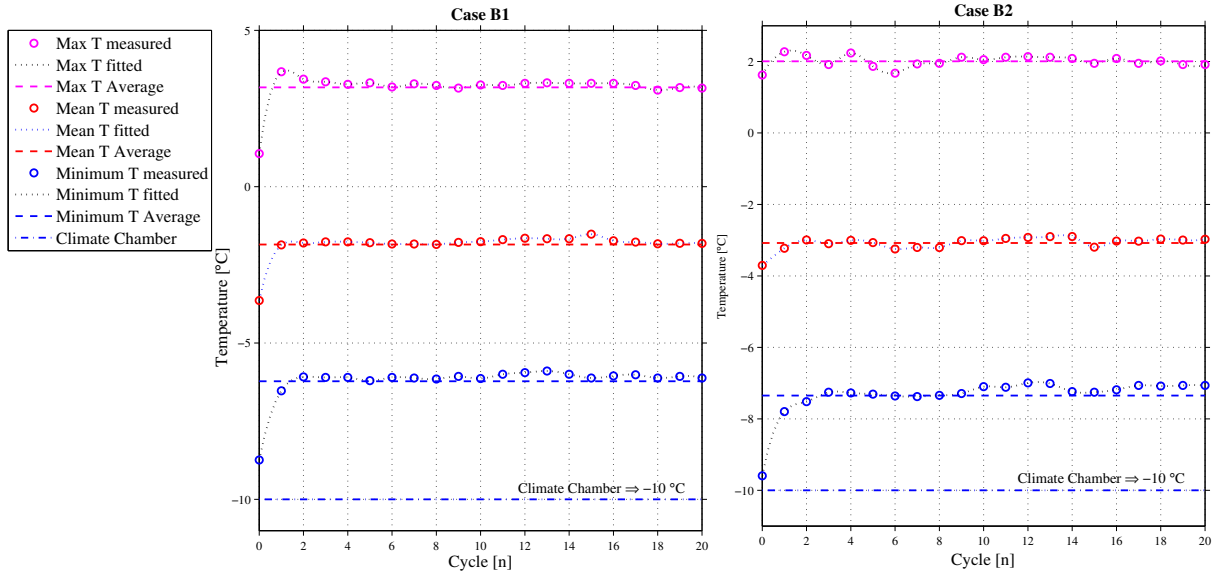
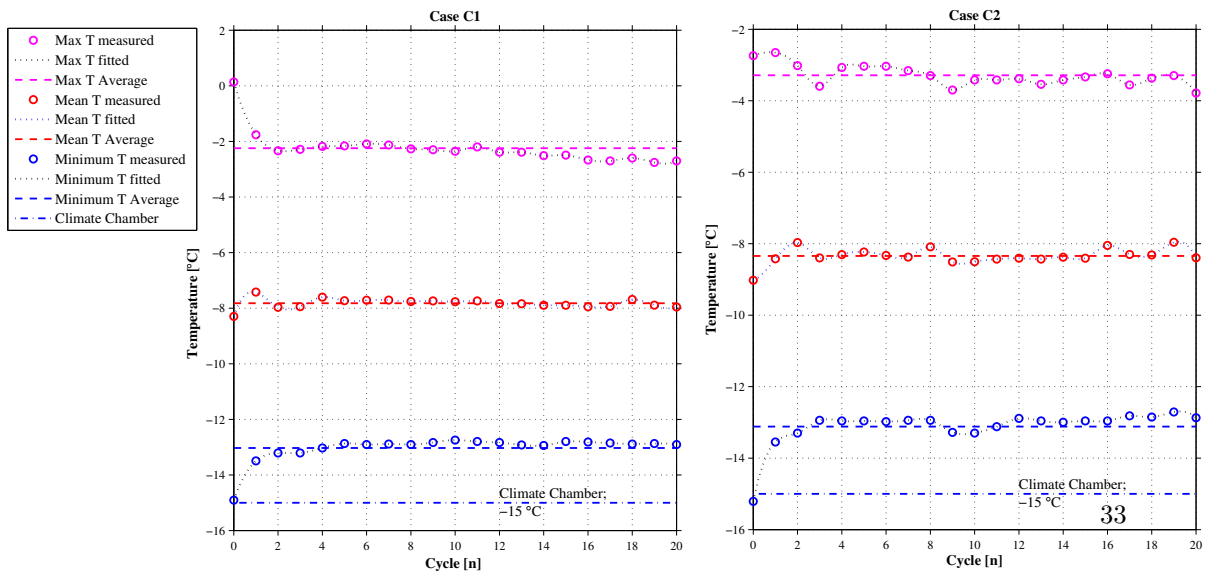


Figure 7.4 Temperature Distribution as a function of Cycle no. for Cases B1 and B2 described in Table 5.3.



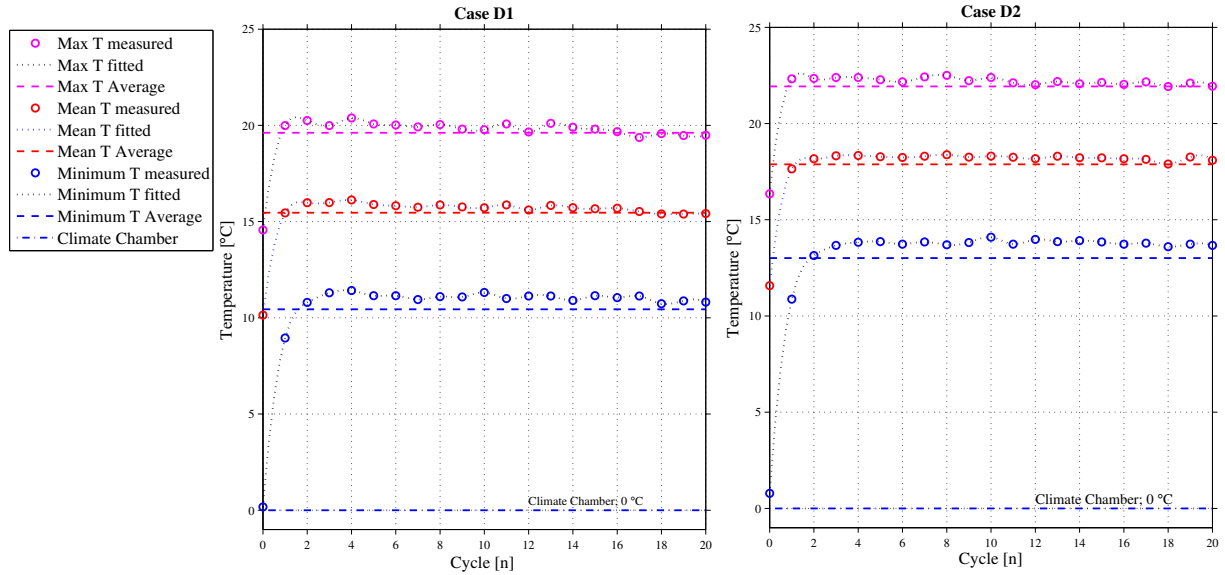


Figure 7.6 Temperature Distribution as a function of Cycle no. for Cases D1 and D2 described in Table 5.3.

7.3 Cycling measurements results: Stress Factor Dependence

7.3.1 Capacity Fading: Temperature dependence

To investigate the influence of low temperature on the capacity, the cells were cycled in the climate chamber at set temperatures mentioned in the Table 5.3. The specifications of the climate chamber are given in Table A.5. The End of Life (EoL) limit is set to the point where the remaining capacity is less than 80%. Figure 7.7 shows the capacity fade for different test cases for different temperatures and C rates. One observation is that each of the two tested cells show a very similar ageing pattern except Cases C1 and C2.

For Cases C1 and C2, the capacity fade was found to be uneven as seen in Figure 7.7 unlike other cases owing to the dramatic self heating of the cells. The capacity with which cells charge and discharge was seen to be heavily affected at this low temperature (-15°C) and a few degrees make a huge difference. Significant degradation can be seen at this charging rate and temperature. According to [30], this may be caused by CC/CV charging method. For Case E1, the test was conducted with a forced air cooling in the climate chamber to keep the cell temperatures close to set temperature. In spite of that, the capacity fade was found to be uneven. It can be inferred that a CC discharge and a CC/CV charge even with active air cooling will not be suitable at this low temperature (-15°C). The work in [30] proposes another charging method to prevent degradation during charging at such low temperatures. An alternative approach of charging could either be CC or CC/CV in both directions. Cycling the cells in a water bath or oil could also be tested to keep the temperature to -15°C since impedance is non linearly depending on temperature. However, this was not tested in this thesis due to time constraints and insufficient availability of channels.

It can also be seen in Figure 7.7 that cells for Cases A1/A2 reached 95% of the nominal discharge capacity after 300 cycles. The average temperature was found to be 5°C. Cells for Cases B1/B2 reached EoL after 125 cycles indicating that cells aged significantly at -10°C and the fade rate is significantly higher. Though the set temperature is -10°C, the average temperature reached was -3°C. Cells in Cases D1/D2 appear not to reach the EoL but the cells reached a very high average cycling temperature of 15°C.

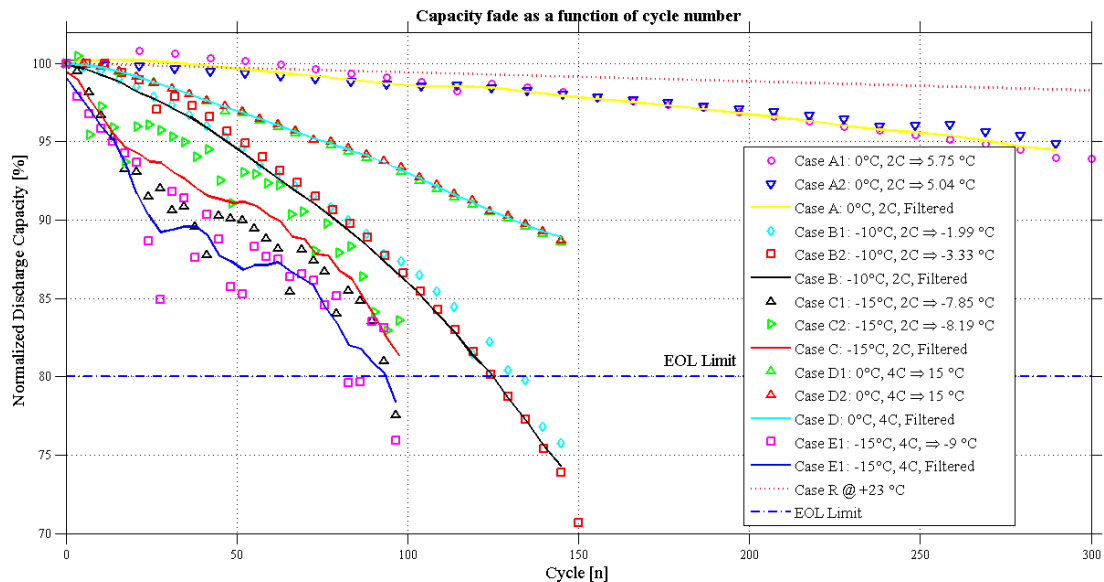


Figure 7.7 Capacity fading as a function of cycle number for cases described in Table 5.3. Dotted red line shows the capacity fade at +23°.

Table 7.1 Average temperatures reached during cycling.

Case	Set Temperature [°C]	Actual Temperature (Average) [°C]
A1	0°C	5.75°C
A2	0°C	5.04°C
B1	-10°C	-2°C
B2	-10°C	-3.33°C
C1	-15°C	-7.85°C
C2	-15°C	-8.19°C
D1	0°C	15°C
D2	0°C	15°C
E1	-15°C	-9°C

7.3.2 Capacity Loss at room temperature

Figure 7.8 shows the actual C/10 capacity loss at a temperature close to room temperature (24°C) as measured from the reference performance tests for different

cases. The broken black line shows the capacity as given by manufacturer. It must be reiterated that the cells in question are four-year old and there is some amount of calendar ageing at BoL.

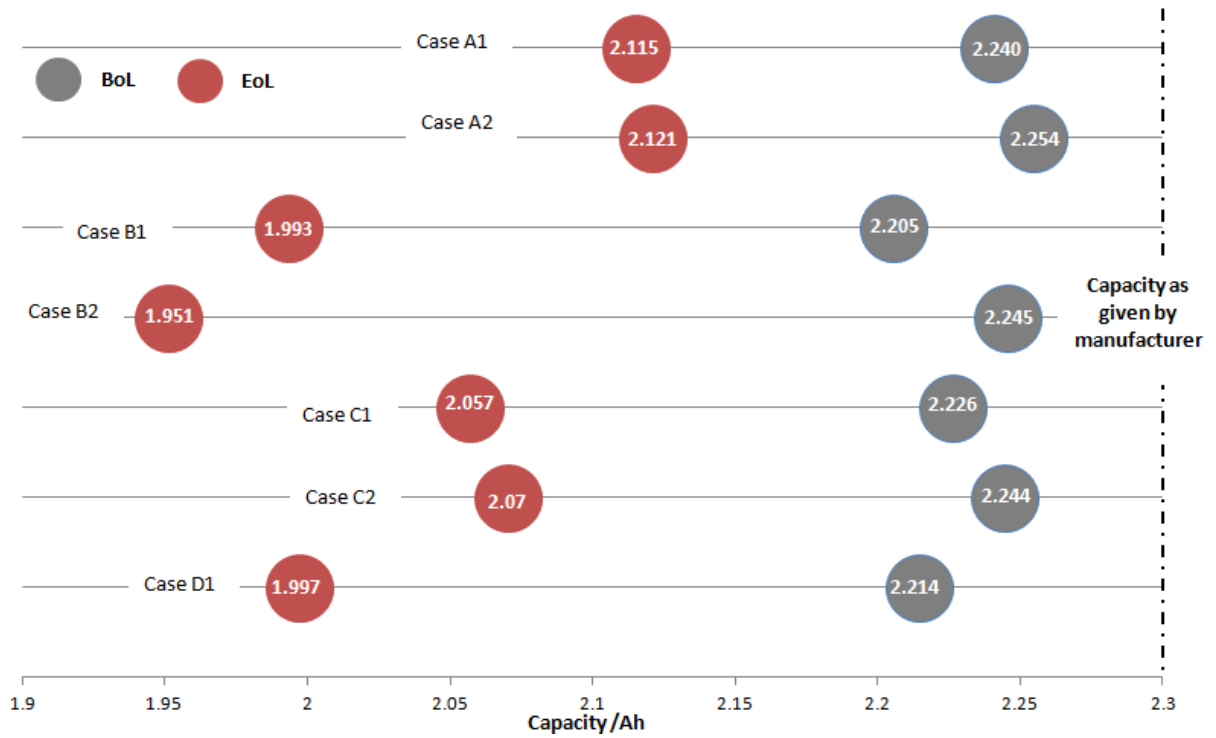


Figure 7.8 C/10 Capacity loss measured on RPTs for individual cases described in Table 5.3 at room temperature.

(Broken black line shows the capacity as given by the manufacturer).

Table 7.2 shows the start capacity, end capacity values as measured for different cases from the RPTs and the number of cycles run for each case.

Table 7.2 Start and End Capacities obtained for different cases at room temperature.

Case	Start Capacity [Ah]	End Capacity [Ah]	Cycles run
A1	2.240	2.115	300
A2	2.254	2.121	300
B1	2.205	1.993	150
B2	2.245	1.951	150
C1	2.226	2.057	100
C2	2.244	2.07	100
D1	2.214	1.997	150

7.4 Comparison of Open Circuit Voltage for different tests

As mentioned in section 5.3, *RPTs* were performed on each cycled cell and The close-to-equilibrium (cte) OCV was determined. Figure 7.9 shows the OCV region obtained from different cycle life tests. The solid blue curve represents the test with

the new battery and others represent the test cases for different temperatures and C rates as mentioned in Table 5.3. Figure 7.9 indicates that the battery ageing has only marginal influence on the shape of the OCV curves if this was plotted against the SoC expressed in %. This indicates that the tested cell has suffered from a net loss of capacity.

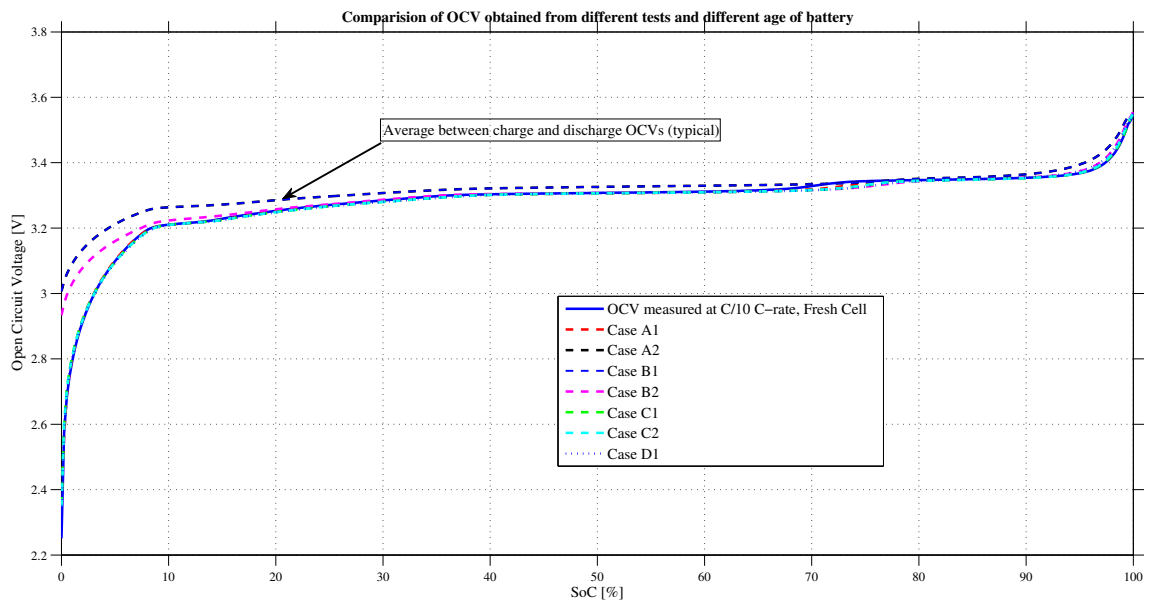


Figure 7.9 Comparison of OCV obtained from different tests and different age of battery.

7.5 Voltage Profiles

This section presents another method of characterising cell ageing mechanism. Charge and Discharge tests at C/1 and C/10 current rate were included in the RPTs in [5] and summarized in Table 5.1.

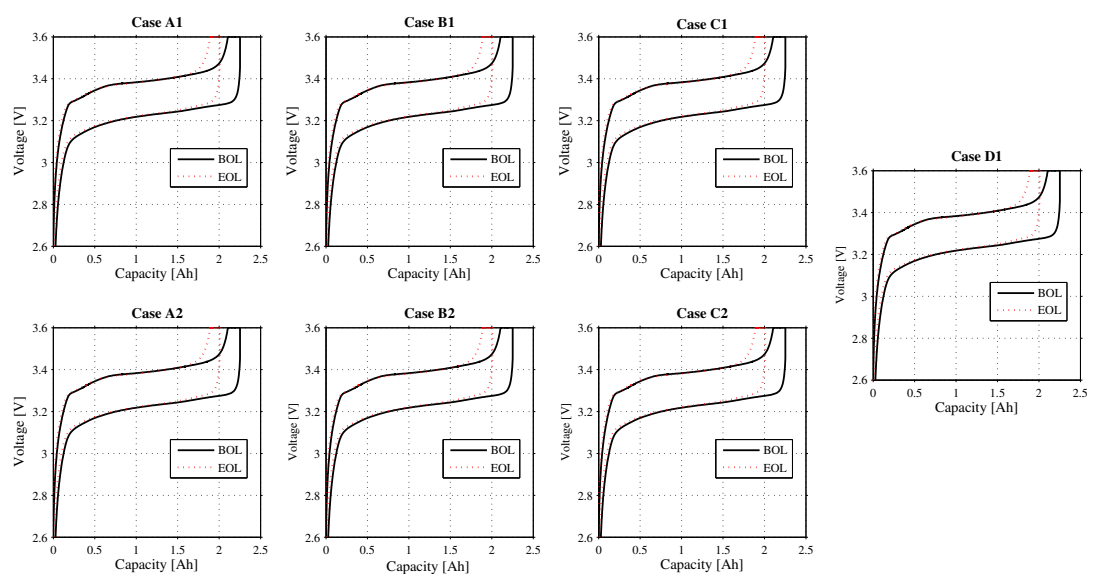


Figure 7.10 C/1 voltage profile vs. capacity for cells for Case A1-D1.

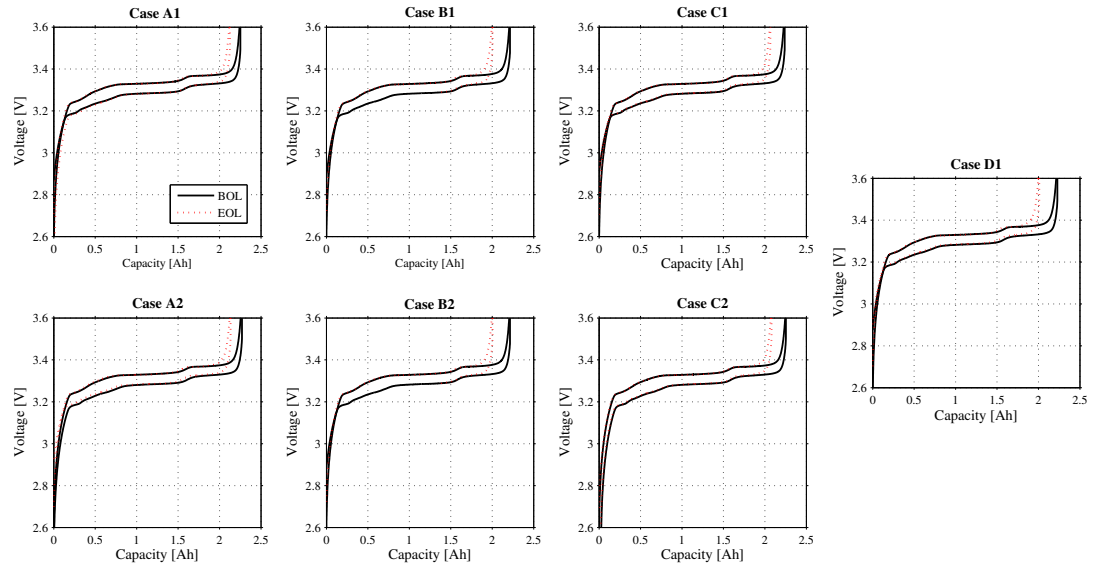


Figure 7.11 C/10 voltage profile *vs.* capacity for cells for Case A1-D1.

Figures 7.10 and 7.11 show the voltage profiles as a function of measured capacity at C/1 and C/10 current rate respectively for test cases A1-D1, showing both the decrease in capacity and change in characteristics of the cell. All the cells for Case A1 to D1 suffer from the same behaviour. For instance, for Case A1 and A2, at BoL, the voltage plateau was long enough but at EoL, the whole curve is compressed which indicates that the anode is ageing. The voltage plateau is disappearing which indicates that the lithium is lost. Most of the capacity loss is related to the amount of lithium that reacts to form the Solid Electrolyte Interphase or Lithium plating and is no longer functional in battery and creating an offset between anode and cathode. There is an initial offset (capacity wise) due to initial SEI formation as shown in Figure 7.12 and that offset grows if the cyclable Lithium is lost or due to lithium plating which means only a lower amount of lithium can be cycled.

The loss in performance can also be ascribed to the uneven degradation of the anode. The dominating mechanism here could be the loss of lithium or possible loss of cathode. It might be difficult to distinguish which mechanism is dominating here but it can either be shrinking of anode or shifting ascribing to the electrode mismatch. Figure 7.10 on the other hand, showing voltage profiles at C/1 current rate, indicates very less impedance growth.

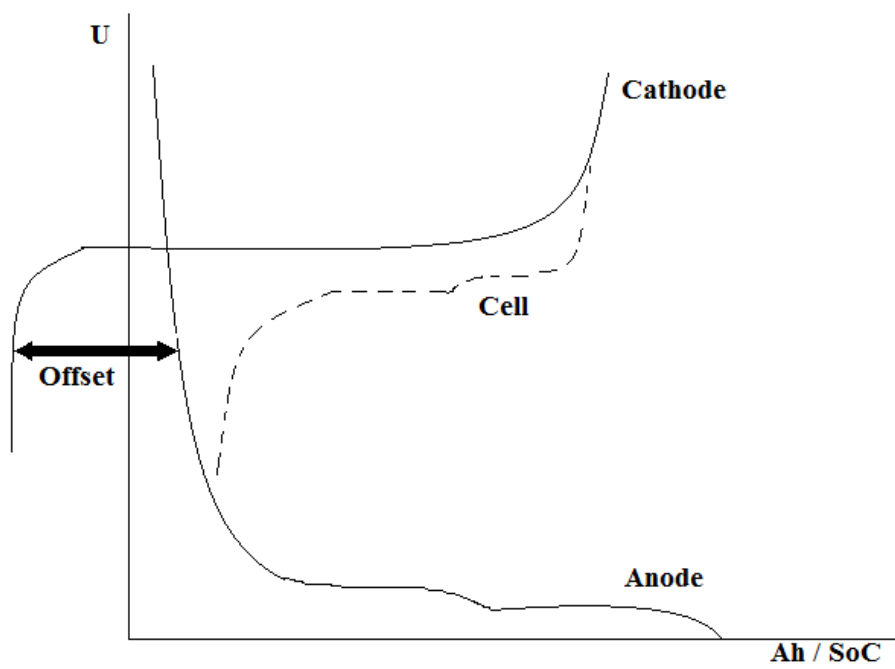


Figure 7.12 Growth in offset due to loss of cyclable lithium.

Chapter 8

Conclusions & Future Work

8.1 Conclusion

The thesis focused on the effect of ageing that low temperature conditions and C-rates have on $LiFePO_4//$ Graphite cells optimized for power applications. Lithium loss or possible loss of cathode was found to be the dominating ageing mechanism for most of the test cases. As expected, a significant reduction in lifetime was observed for cells cycled with a wide SoC range which is known to have a profound effect on ageing. The battery cells cycled using a wide SoC range showed a fast capacity fade before reaching the EoL criteria of remaining capacity of less than 80%.

Further, a CC/CV charge/discharge even with active air cooling was *not* found to be a suitable approach at a low temperature of -15°C due to dramatic *self heating* of the cells. The capacity with which cells charge and discharge is heavily affected by the temperature and a few degrees make a huge difference. The ageing is accelerated at a temperature of -15°C . Further, there are hints that low temperature charging is governed by the properties of the electrolyte ($LiPF_6$ in this case) and it will be interesting to verify if there is electrolyte breakdown condition at this temperature.

The capacity fade trend is linear up to -10°C but at -15°C , the impedance is non-linearly depending on temperature. It can be concluded that temperature is an important factor and at a threshold value of -15°C , the issue of self heating of the cells is encountered. Another charging approach can be adopted to prevent the self heating at this temperature. While the other approach was not tested, the work in [30] gives this indication. A combination of voltage profiles, electrochemical impedance spectroscopy and *OCV* comparison was used to quantify the ageing mechanism.

8.2 Future work

Battery modeling has been in spotlight again due to rise of hybrid electric vehicles (HEVs) and battery electric vehicles (BEVs). Much is still unknown how such vehicles and their battery behave in the long run and what their rest value will be. In future work, improvements can be made by doing a full parametrization at selected

C rates so that the effect of low temperature performance can be better understood and quantified. Different charging approaches can be evaluated to find the optimum method for this particular application. Tests using water bath or oil could be done to keep the temperatures to set temperature.

A *postmortem analysis* (disassembling the cells) on some of the cells can be done to see what actually happened. Low temperature charging in general is governed by the properties of the electrolyte. This should be verified in the *postmortem analysis* if the electrolyte ($LiPF_6$) has broken down rather than functioning accordingly e.g. looking for yellow/brown discolouration of the electrolyte and/or powder-like appearance. The findings on ageing were based on $LiFePO_4$ cells and can be verified for other chemistries. There are many research possibilities at the pack level. Very little research has been conducted on pack level. The lifetime of a battery pack is also greatly influenced by the thermal management of the cells. Hence, a lot of work is still required in battery modeling to characterise and predict the lifetime of HEV batteries.

References

- [1] S. Fletcher, *Bottled Lightning - Superbatteries, electric cars and the new lithium economy*. Hill & Wang, 2011.
- [2] Dirk Uwe Sauer, “Battery Charging – Battery restrictions, needs for charging power, management strategies.” Tutorial PCIM 2013 - Nuremberg, 2013.
- [3] L. Lam, *A Practical Circuit based Model for State of Health Estimation of Li-ion Battery Cells in Electric Vehicles*. Master thesis, Delft University of Technology, Department of Electrical Sustainable Energy, Delft, Netherlands, August 2011.
- [4] E. Prada and M. Petit, “Aging modeling for advanced Li-ion battery pack sizing and management for HEV/EV through AMESim simulation platform,” *LMS Conference*, May 2013.
- [5] J. Groot, *State-of-health estimation of Li-ion batteries: cycle life test methods*. Licentiate thesis, Chalmers University of Technology, Department of Energy and Environment, Gothenburg, Sweden, August 2012.
- [6] H. Yiran, “Electro-thermal battery model identification for automotive applications,” *Journal of Power Sources*, pp. 449–457, June 2010.
- [7] Idaho National Laboratory, “Battery Technology Life Verification Test Manual,” 2005.
- [8] Battery University, “What is the C-rate?.” <http://batteryuniversity.com/learn/article/whatisthecrate>, 2011. [Online; accessed 01-February-2014].
- [9] D. Doerffel, *Testing and Characterisation of Large High-Energy Lithium-Ion Batteries for Electric and Hybrid Electric Vehicles*. Phd thesis, University Of Southampton, Faculty of Engineering, Science and Mathematics, March 2007.
- [10] H. Y. Paul Nelson, Khalil Amine, “Advanced lithium-ion batteries for plug-in hybrid-electric vehicles,” *Argonne National Laboratory*, pp. 440–457, 2010.
- [11] J. G. Bruno Scrosati, “Lithium batteries: Status, prospects and future,” *Journal of Power Sources*, pp. 2419–2430, November 2009.
- [12] D. A. et al, “Design of electrolyte solutions for Li and Li-ion batteries: a review,” *Electrochimica Acta*.
- [13] V. et al, “Ageing mechanism in li-ion batteries,” *Journal of Power Sources*, pp. 269–281, March 2005.

- [14] T. Z. et al, "Aging in lithium-ion batteries: Model and experimental investigation of harvested LiFePO_4 and mesocarbon microbead graphite electrodes," *Electrochimica Acta*, pp. 335–348, November 2013.
- [15] Z. L. et al, "A review of lithium deposition in lithium-ion and lithium metal secondary batteries," *Journal of Power Sources*, pp. 168–182, January 2014.
- [16] Balbuena and Y. Perla B Wang, *Lithium-Ion Batteries : Solid-Electrolyte Interphase*. Imperial College Press, 2003.
- [17] S. et al, "Temperature dependence studies of a.c. impedance of lithium-ion cells," *Journal of Applied Electrochemistry*, pp. 267–273, 2002.
- [18] K. X. S.S. Zhang and T. Jow, "Charge and discharge characteristics of a commercial LiCoO_2 based 18650 li-ion battery," *Journal of Power Sources*, pp. 1403–1409, 2006.
- [19] S. T. et al, "Low-temperature charging of lithium-ion cells part I: Electrochemical modeling and experimental investigation of degradation behavior," *Journal of Power Sources*, pp. 305–316, December 2013.
- [20] N. N. Gao Xiangyang, Zhang Jun, "Transient behaviour modeling and physical meaning analysis for battery," *International Conference on Computer Application and System Modeling*, pp. 383–386, 2010.
- [21] C. F. E.Kuhn and G. Friedrich, "Modeling diffusive phenomena using non integer derivative," *European Phys. J. Appl. Phys.*, pp. 183–190, 2004.
- [22] M. Chen and G. Rincon-Mora, "Accurate electrical battery model capable of predicting runtime and I-V performance," *IEEE Trans. on Energy Conv.*, pp. 504–511, 2006.
- [23] A123, "Nanophosphate®high power lithium ion cell ANR26650m1-b." <http://www.a123systems.com/Collateral/Documents/English-US/A123>.
- [24] U.S. Department of Energy, "Battery test manual for plug-in hybrid electric vehicles." <http://batteryuniversity.com/learn/article/whatisthecrate>, 2008. [INL/EXT-07-12536].
- [25] T. J. S.S. Zhang, K. Xu, "The low temperature performance of lithium-ion batteries," *Journal of Power Sources*, pp. 137–140, 2002.
- [26] R. Kroeze and P. Krein, "Electrical battery model for use in dynamic electric vehicle simulations," *PESC*, pp. 1336–1342, 2008.
- [27] A. K. Suttman, *Analysis of Aging Severity Factors For Automotive Lithium Ion Batteries*. Undergraduate honors thesis, The Ohio State University, Department of Mechanical Engineering, August 2010.
- [28] J. Eriksson, *Optimization and regularization of nonlinear least squares problems*. Phd thesis, Umeå University, Department of Computing Science, June 1996.

- [29] G. F. M. M. C. Forgez, D.V. Do and C. Delacourt, “Thermal modeling of a cylindrical $LiFePO_4$ —graphite lithium-ion battery,” *Journal of Power Sources*, pp. 2961–2968, 2010.
- [30] M. B. K. D. Jürgen Remmlinger, Simon Tippmannb, “Low-temperature charging of lithium-ion cells part II: Model reduction and application,” *Journal of Power Sources*, pp. 268–276, December 2013.
- [31] S. C. Chapra, *Applied Numerical Methods with MATLAB for engineers and scientists*. Mc Graw Hill, 2004.
- [32] G. Watson, *A Fast Algorithm for Nonlinearly Constrained Optimization Calculations*. Springer Verlag, 1978.

Appendix A

Specifications

Table A.1 Cell Specifications.

A123 Cell Specifications	
Manufacturer	A123
Cell Type	Round
Nominal Voltage [Volt/cell]	3.3
Peak Charge Voltage [V]	3.6-3.8
Nominal Capacity [Ah]	2.3
Cathode Material type	$LiFePO_4$
Anode Material	Graphite
Electrolyte	$LiPF_6$ in unspecified solution



Figure A.1 A123 ANR26650, 2.3 Ah Lithium-ion Phosphate battery.

Table A.2 GAMRY Reference 3000 settings.

GAMRY Reference 3000 settings	
Frequency range	0-1 <i>MHz</i>
Compliance voltage settings	0-15 <i>V</i>
Compliance current settings	0-3 <i>A</i>

Table A.3 Digatron Battery tester Specifications.

Digatron Battery tester Specifications	
Model	ZLEG 2-200/100-3z BTS
Voltage range	0-10 <i>V</i>
Current range, charging	0-100 <i>A</i>
Current range, discharging	0-200 <i>A</i>
Line regulation, voltage	approx. 0.01 <i>V</i>
Line regulation, current	approx. 0.1 <i>A</i>
Input resistance, Volt. Meas.	8 <i>kΩ</i>
Thermistor inputs	2

Table A.4 Maccor Battery tester Specifications.

Maccor Battery tester Specifications	
Model	Maccor Series 4000
Voltage range	0-5 <i>V</i>
Current range, charging	0-60 <i>A</i>
Current range, discharging	0-60 <i>A</i>
Number of Channels	16
Control accuracy voltage	ca. 0.01 <i>V</i>
Control accuracy current	ca. 0.01 <i>A</i>
Input Impedance	1 <i>MΩ</i>

Table A.5 Climate Chamber Specifications.

Climate Chamber Specifications	
Manufacturer	ESPEC PU-1 KPH
Temperature Uniformity	$\pm 0.5^{\circ}\text{C}$
Temperature Accuracy	$\pm 0.5^{\circ}\text{C}$
Temperature range	-40°C - +100°C

Appendix B

Test Conditions

Table B.1 Test Conditions for Hybrid EIS.

Test Conditions for Hybrid EIS	
Initial frequency [Hz]	50000
Final frequency [Hz]	0.01
Points per decade	10
AC Voltage [<i>mV</i> rms]	10
DC Current [<i>A</i>]	0
Sample Area [<i>cm</i> ²]	1

Appendix C

Calculations

C.1 Linear Least-Squares Regression

Linear least-squares regression is a method to determine the ‘best ’ coefficients in a linear model for given data set. ‘Best ’ for least-squares regression means minimizing the sum of squares of the *estimate* residuals [31], For a straight line model, this gives:

$$S_r = \sum_{i=1}^n e_i^2 = \sum_{i=1}^n (y_i - a_0 - a_1 x_i)^2 \quad (\text{C.1})$$

The sum of squares of the data residuals is given by

$$S_t = \sum (y_i - \bar{y})^2 \quad (\text{C.2})$$

where \bar{y} is arithmetic mean (the sum of the individual data points (y_i) divided by the number of points n)

C.1.1 R^2 : Coefficient of determination

The coefficient of determination or regression coefficient (R^2) is the difference between the sum of the squares of the data residuals and the sum of the squares of the estimate residuals, normalized by the sum of the squares of the data residuals. It represents the percentage of the original uncertainty explained by the model

R^2 value

To calculate R^2 following formula is used,

$$R^2 = \frac{S_t - S_r}{S_t} \quad (\text{C.3})$$

For a perfect fit, $R^2 = 1$

Appendix D

Open Circuit Voltage

V_{oc} Open Circuit Voltage

Dependent on SoC

$$V_{oc}(SoC) = a_1 e^{-a_2 SoC} + a_3 + a_4 SoC + a_5 e^{\frac{a_6}{1-SoC}}$$

D.1 OCV Model Parameters

Table D.1 The parameter values of the OCV V_{oc} , BoL.

Case	a_1	a_2	a_3	a_4	a_5	R^2
A1	-0.75	0.41	3.26	0	-0.05	0.9582
A2	-0.73	0.41	3.26	0	0	0.9560
B1	-0.72	0.41	3.22	1.77E-003	0	0.9592
B2	-0.74	0.41	3.21	0	0	0.9575
C1	-0.75	0.41	3.22	0	0	0.9569
C2	-0.72	0.40	3.26	0	-0.05	0.9592
D1	-0.74	0.41	3.22	0	0	0.9559
D2	-0.73	0.41	3.22	0	0	0.9571
E1	-0.75	0.41	3.22	0	0	0.9566

Table D.2 The parameter values of the OCV V_{oc} , EoL.

Case	a_1	a_2	a_3	a_4	a_5	R^2
A1	-0.72	0.41	3.26	0	-0.05	0.9594
A2	-0.73	0.41	3.26	0	0	0.9597
B1	-0.24	0.32	3.26	1.36E-003	0	0.8804
B2	-0.27	0.25	3.23	0	0	0.9151
C1	-0.70	0.40	3.22	1.78E-003	0	0.9569
C2	-0.72	0.40	3.22	1.79E-003	-0.01	0.9554
D1	-0.71	0.41	3.22	0	-0.01	0.9559

Appendix E

Proposed Model

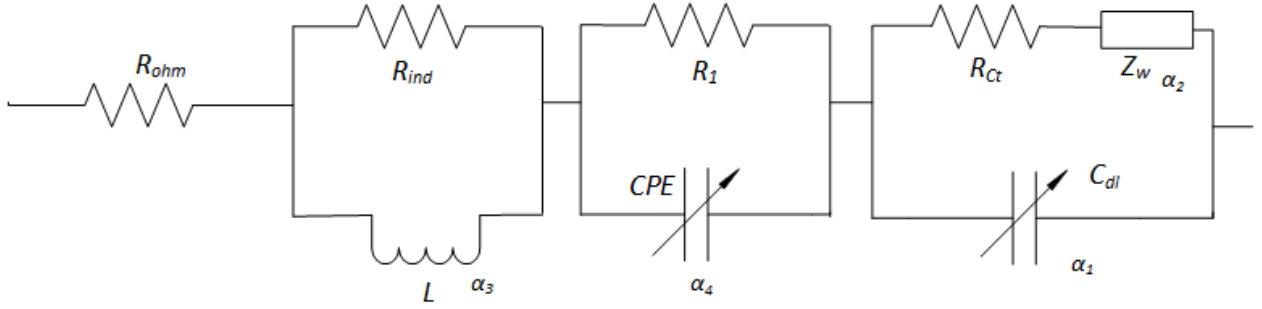


Figure E.1

$$Z_{L_1} = (j\omega_s)^{\alpha_3} L$$

$$Z_L = \frac{Z_{L_1} \cdot R_{ind}}{Z_{L_1} + R_{ind}}$$

$$Z_{dl} = \frac{1}{(j\omega_s)^{\alpha_1} C_{dl}}$$

$$Z_{CPE} = \frac{1}{(j\omega_s)^{\alpha_4} CPE}$$

$$Z_{add} = \frac{R_1 \cdot Z_{CPE}}{R_1 + Z_{CPE}}$$

$$Z_{ct} = \frac{1}{(j\omega_s)^{\alpha_2} Z_w} + R_{ct}$$

$$Z_{sim} = R_{ohm} + Z_L + Z_{add} + \frac{Z_{ct} \cdot Z_{dl}}{Z_{ct} + Z_{dl}}$$

$$\Delta Z_{real} = (Re\{Z_{sim}\} - (Re\{Z_{exp}\})).weight$$

$$\Delta Z_{imag} = (Imag\{Z_{sim}\} - Imag\{Z_{exp}\}).weight$$

$$\Delta Z = (\Delta Z_{real})^2 + (\Delta Z_{imag})^2$$

$$\Delta Z = (Z_{sim} - Z_{exp})^2$$

where

- *weight* is a factor multiplied with the errors to prioritize those optimization variables that seem to be most critical,
- Z_{sim} is the Simulated Impedance,
- Z_{exp} is the Measured Impedance,
- ΔZ_{real} is the difference between real part of simulated and measured impedance multiplied by a chosen weight vector,
- ΔZ_{imag} is the difference between imaginary part of simulated and measured impedance multiplied by a chosen weight vector,
- ΔZ is the total error.

Appendix F

Weighted least-square parameter estimation

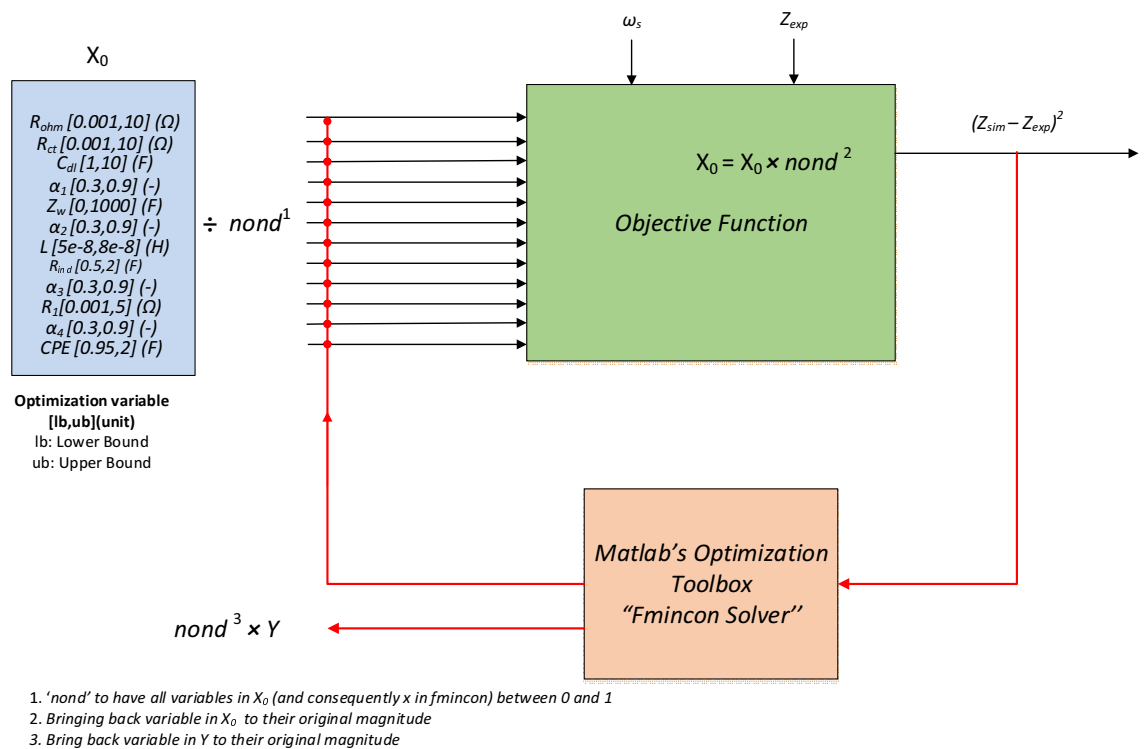


Figure F.1

Figure F.1 shows how the objective function is called by the Matlab's *fmincon* solver which attempts to find a constrained minimum of a scalar function of several variables starting at an initial estimate. This is generally referred to as constrained nonlinear optimization or nonlinear programming [32]. *fmincon* minimizes the error between the experimentally measured impedance and simulated impedance by optimizing the 12 design variables which are subjected to lower and upper boundary value constraints. *fmincon* terminates when a local minimum for the objective function is found giving the optimum value of the design variables. The *interior-point* algorithm was used to solve the problem.

Appendix G

Impedance Based Circuit Model Parameters

Table G.1 Model Parameter values for Beginning of Life for SoC = 20%.

Case	R_{ohm} [Ω]	R_{ct} [Ω]	L [H]	R_{ind} [Ω]	α_3	Z_w	α_2	CPE	α_4	C_{dl} [F]	α_1
A1	0.00104	0.00274	6×10^{-7}	0.83273	0.56	489.1193	0.54	1.219	0.45	4.8273	0.45
A2	0.00056	0.00240	6×10^{-7}	0.83157	0.57	497.0323	0.54	0.982	0.45	5.0316	0.45
B1	0.00139	0.00230	6×10^{-7}	0.7968	0.59	516.44	0.54	1.1462	0.45	4.8471	0.45
B2	0.00126	0.00225	6×10^{-7}	0.7979	0.59	509.49	0.54	1.09	0.45	4.9818	0.45
C1	0.00188	0.001907	5.99×10^{-7}	0.835	0.58	511.843	0.54	1.02	0.45	5.8107	0.45
C2	0.00188	0.002586	6×10^{-7}	0.796	0.59	497.353	0.54	1.529	0.45	4.942	0.45
D2	0.00143	0.0024	6×10^{-7}	0.7989	0.59	522.535	0.54	1.194	0.45	4.7002	0.45

Table G.2 Model Parameter values for End of Life for SoC = 20%.

Case	R_{ohm} [Ω]	R_{ct} [Ω]	L [H]	R_{ind} [Ω]	α_3	Z_w	α_2	CPE	α_4	C_{dl} [F]	α_1
A1	0.00246	0.00335	6×10^{-7}	0.81236	0.57	464.7481	0.54	1.99	0.45	7.5129	0.45
A2	0.00252	0.00034	6×10^{-7}	0.81068	0.59	472.6581	0.54	1.99	0.45	8.2984	0.45
B1	0.00205	0.00180	6×10^{-7}	0.81468	0.59	470.2196	0.54	1.29	0.45	8.9243	0.45
B2	0.00281	0.00183	3.75×10^{-7}	0.85076	0.57	464.9419	0.54	1.49	0.45	8.7352	0.45
C1	0.00224	0.00215	3.75×10^{-7}	0.87293	0.59	474.5891	0.54	1.00	0.45	10.9467	0.45
C2	0.00224	0.00162	6×10^{-7}	0.83759	0.59	476.2342	0.54	0.95	0.45	9.7401	0.45
D2	0.0014954	0.0031634	6×10^{-7}	0.81364	0.59	433.7513	0.54	2	0.45	9.7509	0.45

Table G.3 Model Parameter values for Beginning of Life for SoC = 40%.

Case	R_{ohm} [Ω]	R_{ct} [Ω]	L [H]	R_{ind} [Ω]	α_3	Z_w	α_2	CPE	α_4	C_{dl} [F]	α_1
A1	0.00147	0.00335	6×10^{-7}	0.8317	0.59	542.1924	0.54	1.4511	0.45	4.6077	0.45
A2	0.00152	0.00282	6×10^{-7}	0.8316	0.57	547.061	0.54	1.4765	0.45	5.2237	0.45
B1	0.00219	0.00258	6×10^{-7}	0.7934	0.59	568.0912	0.54	1.7109	0.45	5.052	0.45
B2	0.00196	0.00246	6×10^{-7}	0.7954	0.59	561.9237	0.54	1.51	0.45	5.1147	0.45
C1	0.00224	0.00258	6×10^{-7}	0.8359	0.55	562.55	0.54	0.9507	0.45	5.8428	0.45
C2	0.00224	0.00268	6×10^{-7}	0.79475	0.59759	555.599	0.54	1.853	0.45	5.123	0.45
D2	0.00237	0.0028202	6×10^{-7}	0.7949	0.59831	554.8906	0.54	1.9453	0.45	4.8949	0.45

Table G.4 Model Parameter values for End of Life for SoC = 40%.

Case	R_{ohm} [Ω]	R_{ct} [Ω]	L [H]	R_{ind} [Ω]	α_3	Z_w	α_2	CPE	α_4	C_{dl} [F]	α_1
A1	0.00250	0.00335	6×10^{-7}	0.8115	0.59784	504.7114	0.54	1.9991	0.45	7.3255	0.45
A2	0.00245	0.00334	6×10^{-7}	0.8316	0.57	511.4458	0.54	1.9959	0.45	8.0186	0.45
B1	0.00226	0.00183	6×10^{-7}	0.8137	0.59	505.54	0.54	1.4338	0.45	9.1098	0.45
B2	0.002965	0.0019611	3.75×10^{-7}	0.85013	0.57	491.3664	0.54	1.6563	0.45	9.4	0.45
C1	0.00224	0.00134	6×10^{-7}	0.83926	0.59	541.4998	0.54	0.95022	0.45	7.1487	0.45
C2	0.00224	0.00163	6×10^{-7}	0.83725	0.59	507.916	0.54	0.95001	0.45	9.6523	0.45
D2	0.00159	0.00345	6×10^{-7}	0.81234	0.59	473.9705	0.54	1.999	0.45	10.2306	0.45

Table G.5 Model Parameter values for Beginning of Life for SoC = 60%.

Case	R_{ohm} [Ω]	R_{ct} [Ω]	L [H]	R_{ind} [Ω]	α_3	Z_w	α_2	CPE	α_4	C_{dl} [F]	α_1
A1	0.00114	0.00266	6×10^{-7}	0.83218	0.58	506.8192	0.54	1.2705	0.45	5.0817	0.45
A2	0.00153	0.00282	6×10^{-7}	0.82901	0.50	547.061	0.54	1.4765	0.45	5.2237	0.45
B1	0.00219	0.00258	6×10^{-7}	0.7934	0.59	568.091	0.54	1.7109	0.45	5.052	0.45
B2	0.00196	0.00246	6×10^{-7}	0.7954	0.59	561.9237	0.54	1.51	0.45	5.115	0.45
C1	0.00224	0.00199	5.99×10^{-7}	0.835	0.57	561.608	0.54	1.14	0.45	6.628	0.44
C2	0.00224	0.00268	6×10^{-7}	0.795	0.59	555.599	0.54	1.853	0.45	5.123	0.45
D2	0.00237	0.0028	6×10^{-7}	0.7949	0.59	554.8906	0.54	1.945	0.45	4.8949	0.45

Table G.6 Model Parameter values for End of Life for SoC = 60%.

Case	R_{ohm} [Ω]	R_{ct} [Ω]	L [H]	R_{ind} [Ω]	α_3	Z_w	α_2	CPE	α_4	C_{dl} [F]	α_1
A1	0.00114	0.00266	6×10^{-7}	0.83218	0.58	506.8192	0.54	1.2705	0.45	5.0817	0.45
A2	0.00252	0.00036	6×10^{-7}	0.81059	0.59	462.8714	0.54	1.9985	0.45	8.2534	0.45
B1	0.00203	0.00187	3.75×10^{-7}	0.85335	0.59	437.6609	0.54	0.97058	0.45	9.4109	0.45
B2	0.00146	0.00150	6×10^{-7}	0.81493	0.59	436.5597	0.54	1.0257	0.45	9.3994	0.45
C1	0.00224	0.00129	6×10^{-7}	0.83413	0.59	475.214	0.54	1.0321	0.45	9.7002	0.45
C2	0.00224	0.00124	6×10^{-7}	0.8371	0.59	461.0412	0.54	0.9501	0.45	9.8863	0.45
D2	0.00152	0.00309	6×10^{-7}	0.8133	0.57	427.3704	0.54	2	0.45	9.6844	0.45